DIAGENESIS OF THE ARBUCKLE GROUP IN NORTHEASTERN AND NORTH-CENTRAL OKLAHOMA, U.S.A.

By

PHILLIP ANTHONY BAILEY III

Bachelor of Science in Ocean, Earth, and Atmospheric Sciences

Old Dominion University

Norfolk, Virginia

2011

Submitted to the Faculty of the
Graduate College of the
Oklahoma State University
in partial fulfillment of
the requirements for
the Degree of
MASTER OF SCIENCE
May, 2018

DIAGENESIS OF THE ARBUCKLE GROUP IN NORTHEASTERN AND NORTH-CENTRAL OKLAHOMA, U.S.A.

Thesis Approved:

Jay Gregg, Ph.D.

Thesis Adviser

Jack Pashin, Ph.D.

Jim Puckette, Ph.D.

ACKNOWLEDGEMENTS

This research was funded by AAPG Grants-in-Aid Foundation thanks to the generous award offered by the James Wilson Memorial Fund. I would also like to acknowledge the staff members in the Boone Pickens School of Geology at the Oklahoma State University for their assistance, facilities, and equipment support. Additionally, I would like to thank the Oklahoma Geological Survey Petroleum Information Center (OPIC), Oklahoma City Geological Society Mid-continent Log Library, and the Oklahoma Corporation Commission. All entities played a role in data acquisition. Special thanks to Vyetta Jordan and Jeff Dillon at OPIC for their assistance and hospitality and Ron Clymer at the Corporation Commission for his mentorship and motivation throughout the study.

I would like to my advisor, Dr. Jay Gregg, for his guidance and patience. I would also like to thank my committee members, Dr. Jim Puckette and Dr. Jack Pashin for their continued support throughout my time as a graduate student.

Thanks for the friendship, collegial motivation, and support from graduate students, faculty, and staff at the School of Geology. Special thanks to John Clymer for his assistance in digitizing core observations from literature.

Finally, I like to acknowledge Ashton Bailey (spouse), Colleen Gelormini (mother) and family for their unwavering support.

Name: PHILLIP ANTHONY BAILEY III

Date of Degree: DECEMBER, 2018

Title of Study: DIAGENESIS OF THE ARBUCKLE GROUP IN NORTHEASTERN AND NORTH-CENTRAL OKLAHOMA, U.S.A.

Major Field: GEOLOGY

Abstract: Cambrian-Ordovician age Arbuckle Group carbonates host a wide variety of petroleum, mineral, and freshwater resources in Oklahoma. The studies that have been performed on the Midcontinent have shown the Arbuckle has been affected by both early and late diagenetic events with basinal fluids altering early diagenetic textures. Further constraining the origin, composition, and pathways of basinal fluid flow in northeastern and north-central Oklahoma would allow predictive characterizations of reservoir variability to be made. An integrated petrographic, geochemical, and fluid inclusion microthermometry study of the Arbuckle was performed using four subsurface cores to determine if the Arbuckle was modified by both early fluids (seawater or modified seawater) as well as late diagenetic fluids. The dominant lithology in the Arbuckle is cherty dolomite with interbedded quartz sandstones. Depositional fabrics observed range from subtidal to intertidal facies with some evidence of supratidal deposition. Replacement dolomite observed in all facies exhibit a range of very fine to coarse crystalline, planar to nonplanar textures. Carbon and oxygen isotope data ($\delta^{13}C$ -3.84 to -0.63‰ VPDB and $\delta^{18}O$ -7.92 to -3.08‰ VPDB) indicate much of the replacement dolomite is in equilibrium with early Ordovician seawater (and/or modified seawater) and partially recrystallized during the migration of warm, saline basinal fluids. Void-filling, coarse crystalline saddle dolomite cements plot as more negative $\delta^{18}O$ values (-9.46 to -8.04 ‰VPDB) compared with replacement dolomite. Dolomite cements display a distinctive cathodoluminescent microstratigraphy containing two or more compositional zones. Fluid inclusion microthermometry of dolomite cements display increased homogenization temperatures (> 90ºC). Replacement dolomite and saddle dolomite cements did not display values of $^{87}Sr/^{86}Sr$ in equilibrium with early Ordovician seawater ($^{87}Sr/^{86}Sr$ values ranged from 0.70969-0.71029) and likely indicate interaction with continental basement. This study concludes the Arbuckle Group underwent a complex diagenetic history that began sydepositionally (selected facies), modified by both early (seawater or modified seawater) fluids as well as late diagenetic basinal fluids. The basinal fluids are characterized as warm (90°C-155°C), saline (20-27 wt. % equivalent NaCl) fluids. These fluids are thought to be sourced from the Arkoma and/or Anadarko basins driven by gravity fluid flow mechanisms initiated during or after the Alleghenian/Ouachita orogeny.

TABLE OF CONTENTS

LIST OF TABLES

Table Page

LIST OF FIGURES

Figure Page

dolomite) within laminites in the Gasconade Dolomite (Shads 4). b) Isolated, solution-enlarged vugs are open-filled with saddle dolomite cement and are as large as 7 cm in the longest dimension in the Jefferson City Dolomite (Shads 4). c) Oolitic (grainstone) chert (Shads 4). d) Suspended, rounded, oolitic (packstone-grainstone) chert within a mudstone in the Jefferson City Dolomite (Shads 4). e) Cross-section of a large stromatolite in the Cotter-Powell Dolomite (Shads 4). f) Polygonal-to-globular shaped, centimeter-sized pseudomorphs of gypsum nodules. Wispy, organic seams (mechanically compacted) can be seen draping gypsum nodules (Osage C1; 1cm scale). g) Soft sediment deformation is observed close to the interfaces of sand-rich mudstones and clay-rich, laminated mudstones (Meisner MH 2). h) Stromatolitic 'bump' within cryptmicrobial laminites (left); homogenous, organic-rich mudstone (right; Wichert 1). i) Homogenous, organic-rich mudstone with intermittent laminations (Wichert 1; 5cm scale) 28

Figure 7. *Petrography of replacement dolomite*. a) Very fine-fine crystalline, planar-s dolomite replacing laminated mudstone with occasional, very thin, silty laminations (Shads 4; PPL). b) Very fine-fine crystalline, planar-s dolomite replacing burrowed, pelletal mudstone (Meisner MH 2; PPL); vertical burrow with a slightly coarser crystalline planar dolomite (left) moldic porosity at the top of the vertical burrow (right). c) Micritized peloids-pellets (left), very fine-medium crystalline planar-s to planar-e polymodal dolomite replacing peloidal-pelletal-skeletal wackestone (Meisner MH 2; PPL); pyro-bitumen-filled, sub-horizontal fracture (right). d) Very fine-fine crystalline, planar dolomite replacing cryptmicrobial, 'crinkly' laminites (Meisner MH 2; PPL); organic matter and fine silts were trapped in microbial mats (left). e) Very fine-fine crystalline, planar dolomite replacing organic-rich, laminated mudstones (Wichert 1; XL). f) Fine crystalline, planar dolomite replacing homogenous mudstone (Meisner MH 2; XL). g) Medium to coarse crystalline, planar-e dolomite replacing peloidal, vuggy mudstone (Shads 4; PPL); open vugs can be nearly 1mm in size (left). h) Fine-medium crystalline, planar-nonplanar polymodal dolomite replacing a fenestral carbonate (Shads 4; XL); micritized peloids (left); open pore space

CHAPTER I

INTRODUCTION

This study uses established petrography, geochemistry, and fluid inclusion microthermometry to further the body of knowledge of the diagenetic history of the Arbuckle Group in northeastern and north-central Oklahoma. Specifically, this study tests the hypothesis the Arbuckle Group was modified by both early (seawater derived) fluids as well as late diagenetic basinal fluids in the study area. Using findings from similar studies of the Arbuckle on the Midcontinent, the composition, source(s) and effects of fluid flow events can be constrained.

Arbuckle Group carbonates (Cambrian-Ordovician age carbonates of the Midcontinent) are an economical asset to a number of industries on the Midcontinent (Campbell and Grasmick, 1991; Johnson, 1991; Christenson et al., 2011; Gregg and Shelton, 2012). An estimated 93.8 million tons of base metals (lead, zinc, copper, and other noneconomic metal sulfides) have been mined (Taylor et al., 2009). Mississippi Valley-type (MVT) ore deposits of the Viburnum Mineral District, is one of several mineral districts hosted by Arbuckle carbonates in Southern Missouri. Other mineral districts in the region (including Tri-State Mineral District, Southeast Missouri Mineral District) may have been affected by metalliferous fluids that travelled through the Arbuckle Group (Gregg and Shelton, 2012; King, 2013). Arbuckle Group carbonates also host

significant petroleum reserves on the Midcontinent. In Oklahoma, 129 fields have produced hydrocarbons from Arbuckle reservoirs with the most prolific being the Oklahoma City field, which yielded a maximum flow rate from a single discovery well of greater than 5000 BOPD (Travis, 1930; Campbell and Grasmick, 1991; Johnson, 1991). In addition, petroleum and industrial wastewater disposal (class II Underground Injection Control wells) injected into Arbuckle strata (including the Reagan Sandstone and Precambrian continental basement) have accounted for roughly 51-68% of all disposal in Oklahoma through 2014 (Johnson, 1991; Murray, 2015). The Arbuckle-Simpson and Ozark-Roubidoux aquifers of south-central and northeastern Oklahoma respectively serve as the principal water resource to those regions (Johnson, 1991; Christenson et al., 2011). Other nonfuel mineral resources of Arbuckle Group carbonates have also been mined in Oklahoma (Johnson, 1991).

The correlation between these disposal practices to seismicity in the Midcontinent has increased the need for better understanding the reservoir properties of the Arbuckle Group (Walsh and Zoback, 2015). Researchers have addressed the difficulty of modelling possible seismic hazards without a detailed reservoir characterization and measurements of hydrologic properties (Walter and Zoback, 2015). Documented heterogeneities and a complex diagenetic history of the Arbuckle Group in Oklahoma and Kansas complicates characterization efforts (Temple, 2016; Franseen et al., 2004; Lynch and Al-Shaieb, 1991). Fracture and matrix permeability (horizontal and vertical) in the Arbuckle Group have been shown to be highly heterogeneous and anisotropic (Morgan and Murray, 2015). Using hydrologic properties from measurements hundreds or even tens of kilometers away may not yield reliable predictions in the subsurface. Petrography, fluid inclusion microthermometry, and geochemistry are useful tools in characterizing carbonates with complex depositional and diagenetic histories (Shelton et al., 1992; Goldstein, 2001; Gregg and Shelton, 2012). Studies on the Midcontinent have shown that the Arbuckle was affected by both early and late diagenetic events with basinal fluids altering early diagenetic textures (Gregg et al.,

1993; Temple, 2016; Lynch and Al-Shaieb, 1991, King, 2013; Stoffell et al., 2008; Gregg and Shelton, 1992). Further constraining the origin, composition, and pathways of basinal fluid flow in northeastern and north-central Oklahoma can help predict changes in reservoir variability across the area and increase our understanding of the impact of fluid flow and the evolution of fluids.

All studies of the Arbuckle Group in Oklahoma are limited by the small number and unequal distribution of well penetrations that include publicly available geophysical well logs, core, and other high-resolution data. This is in large part due to the majority of petroleum reservoirs being in the overlying strata.

CHAPTER II

GEOLOGIC SETTING

Oklahoma occupies part of the stable, cratonic interior of North America. Campbell et al. (1991) outlined seven, distinctive geologic provinces in Oklahoma. These geologic provinces are postulated to be indicative of separate hydrological flow units. A transect constructed for this study crosses the Cherokee Platform and Anadarko Shelf leading into the Anadarko Basin (Fig. 1). Major tectonic features in the region include the Ozark Uplift, Arkoma Basin, Nemaha Fault Zone, and Anadarko Basin. The transect (starting in the east) crosses both a westwardly dipping homoclinal platform and the Nemaha Fault Zone, then extends along the Anadarko Shelf and nears the margin of the Anadarko Basin. The Anadarko Shelf is an arcuate homoclinal ramp dipping southward into the Anadarko Basin (Appendix 1). The formation of the Anadarko Basin and other significant tectonic features on the Midcontinent began in the late Proterozoic with younger uplifts occurring throughout the region during Pennsylvanian and Permian Periods (Leach and Rowan, 1986). Heterogeneities in Proterozoic continental basement also indicate multiple igneous and metamorphic terranes underlying the Midcontinent sedimentary cover (Denison, 1981; Chenoweth, 1968; Reeder, 1974). Denison (1981) observed several rhyolitic and granitic basement rock groups in the study area including: Spavinaw Granite Group, Washington County Volcanic Group, and Central Oklahoma Granite Group. Late Paleozoic tectonism along

the Ouachita Thrust Belt is believed to have resulted in northward flow of basinal fluids through lower Paleozoic sediments including the Arbuckle (Benthke and Marshak, 1990; Leach and Rowan, 1986; Viets and Leach 1990). Subsurface faulting in Oklahoma occurs throughout the sedimentary cover and often extend into Precambrian basement (Marsh and Holland, 2016). Observations from fault datasets, in addition to earthquake moment tensor solutions (McNamara et al., 2015; Schoenball and Ellsworth, 2017; Lund Snee and Zoback, 2016), have confirmed that most of the region lies in a strike-slip faulting regime with nearly vertical (70-90°) dipping faults that can extend from one to tens of kilometers in length. The maximum, present day horizontal stress direction is oriented roughly east to west. Many faults are active in Oklahoma as indicated by recent seismicity. Most of the active faults have not been mapped; however, epicenters can delineate lineaments (Schoenball and Ellsworth, 2017). In addition, oil and gas well and seismic reflection datasets show near vertical faults originating in basement and propagating to much shallower depths in younger, Pennsylvanian age formations (Christenson et al., 2011; Bizzell, 2017). In areas where faulting in the Arbuckle Group is observed at the surface (southern Oklahoma, southern Missouri), hydrothermal alteration of host limestone and or dolomites occur (Sargent, 1969; Gentry, 2010; Temple, 2016). Petrographic and geochemical evidence for late diagenetic alteration of Arbuckle age carbonates exists throughout the Midcontinent (Gregg, 1985; Gao et al., 1995; Gentry, 2010; Temple, 2016).

Arbuckle Group carbonates of Cambrian-Ordovician age were deposited on a carbonate platform in an epeiric sea on the stable cratonic interior, which was positioned at roughly 10-25° S latitudes (Palmer, 2012; Fritz et al., 2012). The Arbuckle Group comprises part of the Sauk megasequence and consists of a series of 3rd to 5th order cycles separated by mutliple regional to sub-regional unconformities (Palmer, 2012; Fritz et al., 2012). Depositional environments ranged from supratidal to subtidal and transitioned to an off-platform setting in the southern Oklahoma aulacogen (Gatewood, 1976; Perry, 1989). Paleotopography of the eroded, ‘high relief’ (10’s of

meters) Precambrian basement indicate a 'pock mark' landscape ("Tulsa Mountains") in Rogers and Osage counties (Chenoweth, 1968; Reeder, 1974). Consequently, deposition of carbonates and basal siliciclastic units during the earliest Ordovician transgression may have resulted in locally thicker deposits due to the relief of the paleo-terrane.

There are three documented stratigraphic naming schemes used for Upper Cambrian and Lower Ordovician strata of Oklahoma, Missouri, Arkansas, and Kansas (Chenoweth, 1968; Overstreet et al., 2003). Most of the region recognizes the naming system of McQueen (1931) and McCracken (1955). However, the surface correlation techniques used by these researchers, involving study of insoluble residues, becomes less reliable moving into the subsurface. Cambrian-Lower Ordovician strata in Missouri (and northeastern Oklahoma) do not retain the "group" designation and are indicated by formational names. Despite the lack of a group designation, the term "Arbuckle" in this study will be used for Cambrian-Ordovician strata in the subsurface below the Simpson Group (Fig. 2). Strata included in the Arbuckle Group are temporally equivalent to the Ellenburger Group in Texas, Knox Group of the Appalachian Basin and other "Great American Carbonate Bank" (GACB) carbonate units of North America and elsewhere (Derby et al., 2012). This study will use the Chenoweth (1968) stratigraphic nomenclature in keeping with Derby (1991) and Temple (2016).

The petrology of the Arbuckle has been studied by a number of researchers in eastern and southern Oklahoma, southern Missouri, northern Arkansas, and Kansas in core, outcrop and thin section (He et al., 1997, Overstreet et al., 2003; Franseen, 2004; Lucia, 2012; Fritz et al., 2012; King, 2013; Temple, 2016; Fig. 3). A tabled synopsis of petrographic findings has been included in this report (Table 1). The dominant lithology of the Arbuckle Group in the Ozark Region and northeastern Oklahoma is cherty dolomite. Siliciclastic deposition is interpreted to have been extensive during the early Ordovician and sourced from extrabasinal origins (Overstreet et al. 2003). Major siliciclastic units include the Gunter Sandstone Member at the base of the

Gasconade Dolomite (Ordovician) and the Reagan Sandstone (Cambrian, Oklahoma) and its equivalent Lamotte Sandstone (Cambrian, Missouri; Derby, 1991; Overstreet et al., 2003; Palmer et al., 2012; Fritz et al., 2012). The upper portion of the Reagan Sandstone is equivalent to the Bonneterre Dolomite in Missouri (Chenoweth, 1968). The Arbuckle Group is comprised of six formations (Fig. 2); however, the completeness of the section will vary depending on the locality (Chenoweth, 1968).

The cyclical nature of facies stacking patterns in Cambrian-Ordovician tidal flat successions of the Arbuckle section in southern Missouri and northeastern Oklahoma are well documented (Overstreet et al., 2003; Fritz et al., 2012). Multiple 3rd order sequences and unconformities are observed in the section, notably at the basal and upper contact with Precambrian basement and Middle-Late Ordovician strata of the Simpson Group (Palmer et al., 2012; Fritz et al., 2012;). Between 3rd order unconformities are meter-scale 4th and 5th order cycles that have a range of interpreted depositional environments ranging from subtidal to supratidal consisting of peloidal wackstones-mudstones, stromatolites, ooid grainstones, burrowed mudstones, thrombolite boundstones, microbial laminites, and quartz sandstones (He et al., 1997; Overstreet, 2003; Palmer et al., 2012; Fritz et al., 2012). There are two dominant types of cycles observed in the Ozark Region. Type I cycles are less than 2 meters in thickness and have supratidal caps overlying intertidal-supratidal deposits. Type II cycles are 2-4 meters in thickness and have a thicker subtidal section underlying a intertidal-supratidal section (Overstreet et al., 2003). The supratidal facies typically display evidence of subaerial exposure such as mudcracks, halite casts, and chalcedonic chert nodules with similar shapes as gypsum and anhydrite nodules (Overstreet et al., 2003; Fritz et al., 2012; Temple, 2016). There is evidence for the Arbuckle facies to be similar to both modern tidal-flat analogs of Andros Island, a model for tidal-flat deposition under humid conditions, and Persian Gulf Coast, a model for tidal-flat deposition under arid conditions (Fritz et al., 2012).

Periodic subaerial exposure during Arbuckle deposition resulted in karst development (Lynch and Al Shaieb, 1991; Overstreet et al., 2003). Lynch and Al-Shaieb (1991) documented that 12 of the 30 Arbuckle cores that they examined, mainly from southern and eastern Oklahoma, had macroscopic evidence of karst development. Recognition of subaerial exposure as viewed in core from this study (Shads 4) and others is confined to the easternmost part of studied region (Derby, 1991; Lynch and Al-Shaieb, 1991; Fritz et al., 2012). Lynch and Al-Shaieb (1991) concluded much of the karst development in the Arbuckle may have occurred syndepositionally although several phases of karst are presumed to have occurred later in the Ordovician and Pennsylvanian Periods (Fritz et al., 2012). Fritz et al. (2012) described several phases of karst development that contributed to multiple episodes of dissolution, dolomitization, and cementation including: intra-Arbuckle karst, intra-Simpson karst, sub-Woodford karst, Pennsylvanian karst, and hydrothermal karst. Each subsequent period of karst development may have aided in further enhancing subsurface dissolution features and sinkhole development where 'deeper' Arbuckle formations (Gasconade and Eminence Dolomite) hosted aquifer systems leading to the development of caverns (Dillon et al., 1998).

Reservoir development of the Arbuckle has been shaped from early through late diagenesis and resulted in multiple porosity generation events (Fritz et al., 2012). Initial, primary porosities of the Bonneterre Dolomite in the Viburnum Trend ranged from 6-24% depending on primary lithologies (Gregg et al., 1993). Tectonism during the Pennsylvanian and Permian facilitated the creation of extensive fracture and fault systems. Synchronous or subsequent fluid flow event(s) likely spurred the precipitation of late diagenetic void-filling cements. The stratigraphy of Arbuckle strata, dictated by the cycle stacking architecture, likely influenced reservoir development (Franseen et al., 2003; Fritz et al. 2012). Stacking patterns capped by more porous, lithologies may explain the variability of fluid movement through Arbuckle strata laterally and in the vertical section (Moñtanez and Read, 1992; He et al., 2002; Ahr, 2008; Gregg et al., 2012).

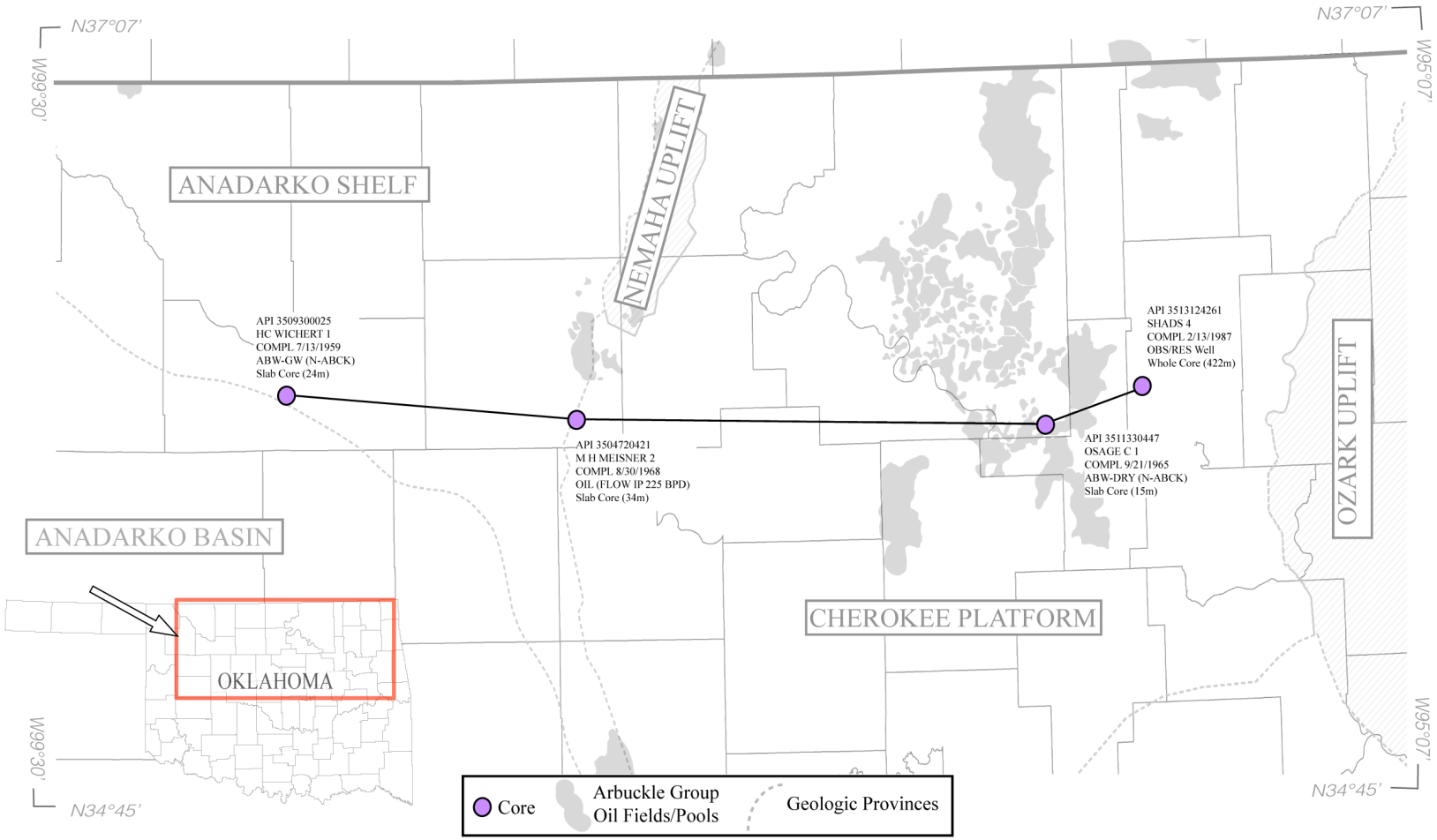

Figure 1. *Study area with core locations and tectonic features*. The transect of cores used in this study crosses the Cherokee Platform and Anadarko Shelf leading into the margin of the Anadarko Basin. Geologic provinces were digitized after Campbell (1991).

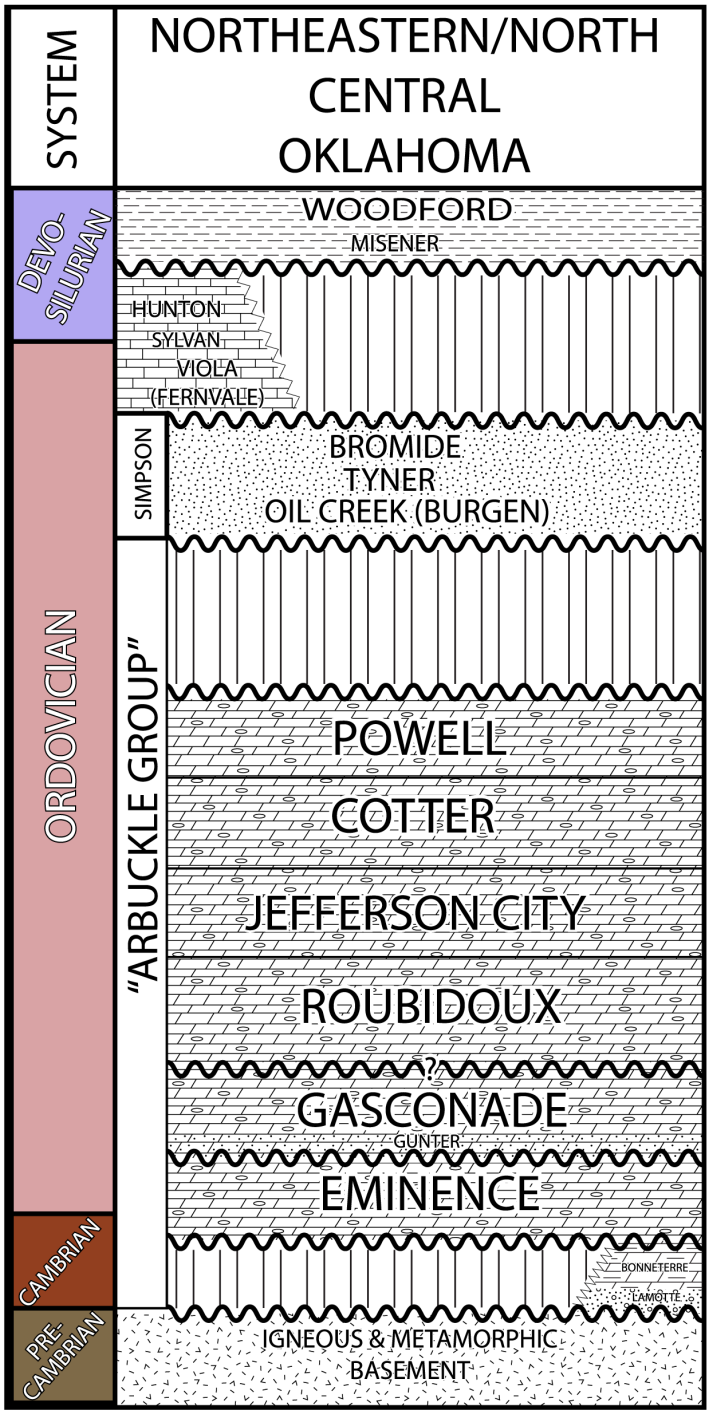

Figure 2. *Stratigraphic column of northeastern and north-central Oklahoma*. The Arbuckle Group is late Cambrian to early Ordovician in age and overlies early-mid Cambrian strata of the Bonneterre Dolomite and Lamotte Sandstone (when present) and underlies the mid-late Ordovician Simpson Group. Pictorial representation of lithology and System colors use USGS standards (modified after Chenoweth, 1968).

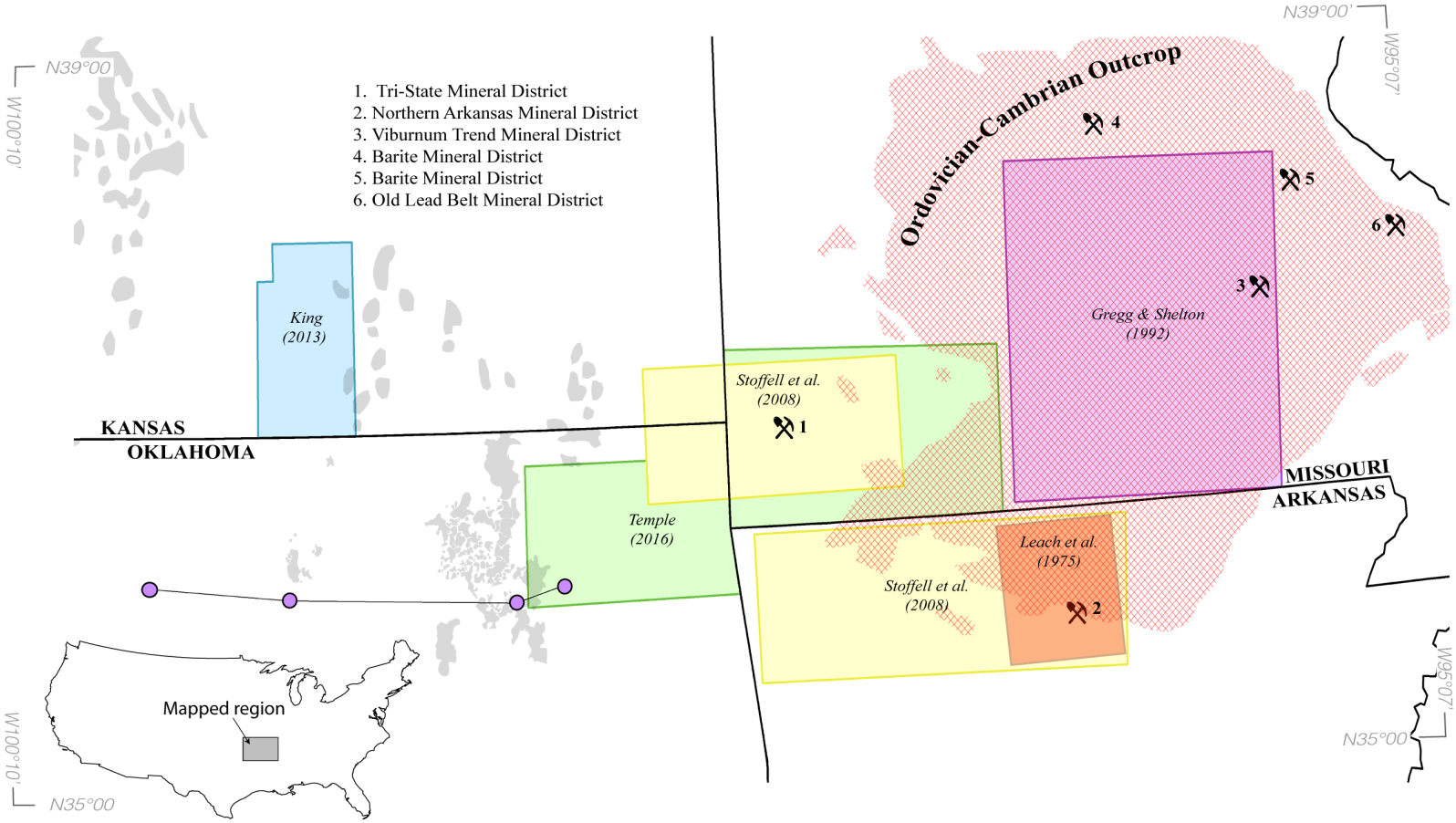

Figure 3. *Previous Arbuckle study area 'footprints' on the Midcontinent*. Similar petrographic and geochemical studies of the Arbuckle have been performed in northeastern Oklahoma, southern and central Missouri, northern Arkansas, and southern Kansas. The data collected in this study extends the body of petrographic and geochemical knowledge of the Arbuckle Group in Oklahoma.

		Temple, 2015 (SW Missouri and NE Oklahoma)		Palmer et al., 2012 (southern Missouri)		Franseen et al., 2004 (Kansas)	
Age	**Formation**	**Facies and/or Lithology (if described)**	**Dolomitic Textures**	**Facies and/or Lithology (if described)**	**Dolomitic Textures**	**Facies and/or Lithology (if described)**	**Dolomitic Textures**
Ordovician	***Cotter/Powell***	Burrowed wackestone and mudstone capped by ooid grainstone and microbial laminites with intercalated thin beds of green shale. Some quartzic sandstone. Some evidence for evaporites at cycle tops (molds of hopper halite crystals and ghosts of gypsum laths).	Light gray to light brown, medium to fine crystalline cherty dolomite.	Cherty dolomite* same as Temple. Oolitic chert and large silicieous ooliths. Brown quartzose oolitic chert.	Light gray to light brown, medium to fine crystalline cherty dolomite.	[Not distinctly separable in outcrop] Coarsely granular, cherty crystalline carbonate (dolomite) with oolitic chert (white and decreases towards base) and tripolitic chert.	Not described or studied.
	Jefferson City	Cherty dolomite containing gypsum and halite casts at cycle tops. Peloidal/burrowed wackestones overlain by microbial laminites and/or ooid grainstones.	Light gray to light-dark brown, medium to fine crystalline, planar-s to planar-e cherty dolomite and argillaceous dolomite. Pink saddle dolomite cement filling open space. Fine crystalline planar-s dolomite (microbial laminite).	Oolitic chert, lenses of orthoquartzite, conglomerate, and shale locally present. Burrowed mudstone.	Light brown to brown, medium to fine crystalline dolomite and argilaceous dolomite. Thick to massive bedded brown medium crystalline dolomite.		
	Roubidoux	[Mixed carbonate siliciclastic system] Meter scale sandstone beds with alternating meter scale dolomite beds. Sandstone is fine to medium grained, subrounded quartz. Dolomite beds with banded brown to gray oolitic chert. Light gray, mottled dolomite and white sandy dolomite overlain by dolomitized microbial laminites. Scattered coaresly crystalline pyrite in vugs.	Light gray to brown dolomite. Fine to medium crystalline, planar-s to planar-e and nonplanar textures containing scattered well to sub-rounded quartz grains. Fractures and vugs lined with coarsely crystalline saddle dolomite cement.	Chert to sandy crystalline carbonate with some dolomitic sandstone-sandstone (quartzose). Sandstone is fine to medium grained, sub-rounded and frosted quartz sand. Brown to gray, banded, oolitic, sandy chert. Sandstone can contain well-preserved rippple marks, mud cracks and cross bedding.	Light gray to brown, fine crystalline, thin tho thick bedded.	Sandy, crystalline carbonate (dolomite) and fine-grained sandstone.	
	Gasconade	Gray, mottled, banded, cherty (chalcedonic) dolomite. Burrowed wackestone/mudstone capped by microbial laminites.	Medium crystalline dolomite, mostly nonplanar dolomite with white to light gray chert to coarse crystalline dolomite. Coarse cystalline dolomite cement filling vugs.	Crystalline carbonate with variable chert content.	Cherty dolomite, medium to coarse crystalline. Variable chert content.	Cherty, coarsely, granular crystalline carbonate (dolomite). Dense, dark-bluish-gray chert in upper part that grades into white, dense, quartzose chert.	
	Gunter Sandstone	Gray to white, sub-rounded sandstone. (syntaxial quartz overgrowths)					
	Eminence	Gray, mottled, banded dolomite with small chert nodules and angular chert fragments. Microbial laminites overlying burrowed wackestone/mudstone.	Medium to coarse crystalline, planar-s and nonplanar dolomite. White silicifed ooids present (upper unit).	Interbedded brown and gray crystalline carbonate (rather undifferentiated).	Medium to massive bedded, light gray, medium to coarse grained dolomite. Small amounts of nodular or angualr chert fragments. Druse quartz. Locally large chert boulders and blocks.	Cherty, buff to white, very coarsely crystalline, crystalline carbonate dolomite. Vitreous semitranslucent chert with finely crsytalline quartz in cavities. (very cherty dolomite)	
	Potosi	Gray, mottled, banded dolomite with small chert nodules and angular chert fragments. Microbial laminites overlying burrowed wackestone/mudstone.	Medium to coarse crystalline, planar-s and nonplanar dolomite.	Mostly undifferentiated crystalline carbonate. Thrombolitic-stromatalitic laminates.	Massive to thickly bedded, medium to fine crystalline dolomite with abundance of druse quartz.	Not described or studied.	
Cambrian	***Derby-Doerun***	Not described or studied.		Dolomitic ribbon rock, mudstone-wackestone interbedded ooid-skeletal packstone-grainstone, locally cross-bedded ooid grainstones, thrombolite and stomralite boundstones. Low chert content.	Brown to gray dolomite, medium to fine crystalline, buff to brown, argillaceous and silty.		
	Davis			Mixed clastic-carbonate unit containing: gray-green, bluish shales, carbonate-cemented quartzose siltstones and fine-grained, locally cross-laminated, riple laminated or burrowed sandstones (variably glauconitic), and clastic-rich limestones (variably dolomitized) and oolitic-fossilieferous-intraclastic limestones.			
	Bonneterre Dolomite			Thin fine-grained limestone to dolomite, thick ooid and skeletal packestones-grainstones, thromolite and stromalites, coarsely crystalline light-gray, tan dolomites. Dolomitized to undolomitized glauconitic limestone with thinly interbedded shale.	Light gray, medium to finely crystalline medium bedded dolomite.		
	Lamotte Sandstone			Sandstones, arkoses, conglomerates, clay-matrix rich sandstone and conglomerates, shale-rich facies. May be locally haemetitic and contain muddy red beds. Overlain quartzitic, burrowed, cross-bedded sandstones locally interbedded with fan-delta deposits (nearby Precambrian highs)			

Table 1. *Selected Arbuckle petrographic findings on the Midcontinent.*

CHAPTER III

METHODS

Four subsurface cores of the Arbuckle Group were viewed and sampled at Oklahoma Geological Survey Petroleum Information Center (OPIC) in Norman, Oklahoma. The cores range from 24m to 422m in length and lie along a section from northeastern to north-central Oklahoma (Fig. 1). Original copies of wireline logs were obtained for each well in the study from the Oklahoma City Geological Society Mid-Continent Library ("Log Library") and converted into raster and Log ASCII Standard (LAS) files for only the Arbuckle Group interval. The logs were used for lithostratigraphic correlations using Information Handling Services (IHS) Kingdom software. Wireline curves used for correlation included: gamma-ray (GR), spontaneous potential (SP), and resistivity (RES). Arbuckle Group formation tops collected from IHS Enerdeq Online Database Browser were used as the initial formation top picks and refined using top calls from Brizendine (2016). The top of the Arbuckle Group was used as the datum for building the cross section.

Thirty-eight core samples were cut into approximately 5cm x 5cm x 0.6cm billets. Core sample selection was based on collecting representative facies, identification of void-filling cements, and host carbonate rock. Petrographic analysis was conducted on thirty-eight thin sections made from these samples at Oklahoma State University. Thin sections were prepared by Quality Thin

Sections based in Tucson, Arizona. Cathodoluminescence (CL) petrography was carried out using a CITL CL8200 MK5-1 cold cathode optical CL system mounted on an Olympus BX 41 microscope equipped with 4X, 10X, and 40X long focal distance objective lenses, and a "Q-imaging" 5-megapixel cooled, low-light, digital camera system.

Carbon and oxygen isotope compositions were measured at the University of Miami Stable Isotope Laboratory using a Finnigan-MAT 251 mass spectrometer. Standard error was reported relative to the Vienna Pee Dee Belemnite (VPDB) standard for $\delta^{13}C$ and $\delta^{18}O$ and was less than ±0.08‰ based on replicate measurements (Swart and Eberli, 2005). All samples were reacted for 10 minutes using the common acid bath method at 90˚C and standard isobaric corrections were applied. Corrections were not applied for the differences in the fractionation of $\delta^{18}O$ as a result of the dissolution of dolomite by phosphoric acid (Swart et al., 2005). Ratios of $^{87}Sr/^{86}Sr$ were measured using a Thermal Ionisation Mass Spectrometry (TIMS) at the University of Kansas Radiogenic Isotope Laboratory and have errors of 0.000014 at 95% confidence level.

Fluid inclusion microthermometric measurements were performed on eight, doubly polished thick sections at Oklahoma State University. Thick sections were prepared using techniques designed to avoid extensive heating of samples (Goldstein and Reynolds, 1994). Measurements were made using a Linkam THMSG 600 heating and cooling stage. Errors of homogenization (T_h) and last ice melting (T_m) temperatures were ±1.0˚C and ±0.3˚C, respectively based on analysis of synthetic fluid inclusions (Shelton and Orville, 1980). Inclusions analyzed in this study were aqueous, two-phase, primary inclusions, using the classification of Roedder (1984). T_m measurements were used to calculate salinities using equations from Bodnar (1992).

CHAPTER IV

RESULTS

Electric Log Correlation

All four cores were correlated using the top of the Arbuckle initially using IHS Enerdeq formation top data and refined following Brizendine (2016) using the following curves: spontaneous potential (SP), gamma-ray (GR), and resistivity (RES) logs, if available. Using the Shads 4 core as the primary type log for Arbuckle Group formations, it was determined the Osage C-1 core sampled the basal Gasconade Formation (Gunter Sandstone Member), and both the Meisner MH 2 and Wichert 1 cores sampled the Cotter-Powell and/or Jefferson City Formations (Fig. 4). Correlations were based on lithostratigraphic correlations for purposes of identifying cored intervals.

Stratigraphy and Petrology

Four subsurface cores (whole and discontinuous slab) of Arbuckle strata in Oklahoma were studied including (from east to west): Shads 4, Osage C-1, Meisner MH 2, and Wichert 1 (Fig. 1). One of the oil wells, Meisner MH 2, cored, tested and produced from the 'upper' Arbuckle, with an initial oil production (41.5° gravity oil) of 225 BPD on a 32/64" choke. The Shads 4 core was the focus of the study because it cored a complete Arbuckle Group section of 422m. Work done

by James Derby (1991) was heavily relied upon for formation top calls in addition to a full lithology description with sub-meter scale resolution. The lithological descriptions by Derby (1991) were digitized and are included in Appendix 2. Only 15 m of 'basal' Arbuckle, 34 m of 'upper' Arbuckle, and 24 m of 'upper' Arbuckle are represented in the Osage C-1, Meisner MH 2, and Wichert 1 cores respectively. Details of these oil and observation wells are included in Appendix 3. Correlations of Arbuckle Group formation tops were interpreted in cross section (Fig. 4).

All cored intervals were observed to be dolomitized based on petrography and a weak effervescence in diluted hydrochloric acid. Core and thin section descriptions start at the base of each formation. Core examination was done at a sub-meter scale. Tabled core descriptions are included in Appendix 4.

The Shads 4 core (Fig. 1) has 422m of continuous core of the complete Arbuckle section from 493 m to 895 m (Fig. 5). Precambrian basement of the Washington Volcanic Group was cored with predominantly reddish-brown, andesite porphyry. A nonconformable contact exists between the Reagan Sandstone Formation and Precambrian, Washington Volcanic Group. The Reagan Sandstone (896-918 m) is comprised of light to dark brown, arkosic sandstones with interbedded, thin shale beds. No distinct differences were observed in the Reagan Sandstone compared to the Lamotte Sandstone in southern Missouri as described by Palmer et al. (2012). If the Lamotte Sandstone is the age-correlative formation to the Reagan Sandstone, the Reagan is the only Upper Cambrian strata examined in this study. Previous authors have noted an unconformable contact that exists between Upper Cambrian carbonates and the Gasconade Dolomite (Overstreet et al. 2003; He et al., 2012). Derby (1991) described a "pebbly, weathered disconformity zone" close to the suggested unconformity.

The Gunter Sandstone Member (863-896 m) at the base of the Gasconade Dolomite is a mix of gray to white, medium-grained, sub-rounded sandstone, sandy dolomite, burrowed dolomitic mudstone and shale. Palmer et al. (2012) described the composition of the Gunter Sandstone in southwestern Missouri as being made up of several meter-scale shoaling-upward cycles. While cyclicity at that resolution was not specifically observed or documented in the Gunter Sandstone, shoaling-upward cycles are thought to be present given the range of facies that were observed. Facies include: burrowed-mottled mudstones, laminated mudstones, shales, and quartz sandstones. Sandstone facies typically have intergranular porosity up to 5-10% (visually estimated). Burrowed-mottled, dolomitic mudstones displayed intercrystalline porosity up to 5-10% (visually estimated). Isolated, solution-enlarged vugs are open to filled with nonplanar (saddle) dolomite cement crystals as large as 4 cm in the longest dimension. Sulfide mineralization (pyrite, sphalerite, and galena) is present in thin (<0.25 m) vuggy zones.

The Gasconade Dolomite (797-863 m) is dominantly thick (>2 m) intertidal to subtidal 4th to 5th order paracycles consisting of gray to brown, medium crystalline, cherty dolomite. The Gasconade is composed of brown to gray silicified, burrowed dolomitic mudstones, pelletal-skeletal packstones, microbial laminates and hemispherical stromatolites. Primary porosity is intercrystalline with secondary porosity types consisting of moldic, fracture, fenestral, and vuggy porosity up to 5-20% with extremely vuggy zones displaying >20% porosity (visually estimated) (Fig. 6a). The secondary porosity types observed are more typically found in the packstone facies. Extremely vuggy zones (>0.25 m in thickness) exist in the Gasconade and are 2 cm high extending across the core with some intervals of quartz-lined vugs. Oil staining exists near the base.

The Roubidoux Formation (725-797 m) is comprised of thick (>2 m) intertidal 4th to 5th order paracycles consisting of bedded gray, cherty to sandy dolomite, planar stromatolites, thrombolitic dolomite, and dolomitic sandstone as observed by Palmer et al. (2012). Primary porosity is

intercrystalline with secondary porosity types consisting of moldic, fracture, fenestral, and vuggy porosity up to 5-20% (visually estimated). Chert and sand concentrations vary throughout the section; however, sand content decreases overall up-section and transition to mainly cherty dolomite. Zones of brecciated chert and thin chert nodules are less prevalent in the upper part of the formation. Vugs are scattered throughout.

The Jefferson City Dolomite (616-725 m) is comprised of brown to gray, cherty dolomite with shoaling upward cycles of dolomitic mudstones-wackestones overlain by pelletal or oolitic packstones/grainstones and stromatolites. Primary porosity is intercrystalline with secondary porosity types consisting of moldic, fracture, and vuggy porosity up to 5-20% (visually estimated). Isolated, solution-enlarged vugs are open to filled with saddle dolomite cement and are as large as 7 cm in the longest dimension (Fig. 6b). Thin zones of dissolution breccia and chert nodules exist at 4th to 5th order cycle tops as observed by Overstreet et al. (2003). The base of shoaling upward cycles is typically oil stained. Cycle tops of oolitic packstones/grainstones are partially to fully replaced by chert and also display bitumen staining. Oolitic chert is commonly observed in intertidal facies, most notably in oolitic packstones and grainstones (Fig. 6c). Rarely, suspended, rounded oolitic chert clasts (2-3cm) occur within subtidal facies (Fig. 6d).

The Cotter and Powell Dolomites (493-616 m) are cyclic light gray to gray to brown, cherty, burrowed-mottled, laminated, dolomitic mudstones-wackestones overlain by stromatolites and oolitic packstones-grainstones. A large (>10 cm in diameter), hemispheroidal stromatolite was observed in the section (Fig. 6e). Primary porosity is intercrystalline with secondary porosity types consisting of moldic, fracture, and vuggy porosity up to 5-20% (visually estimated). Chert partially or fully replaced oolitic packstones/grainstones facies. Brecciated zones were more prevalent than in the rest of the entire Arbuckle section. These zones were found at 4th and 5th order cycle tops in the Cotter and Powell Dolomite as observed by Overstreet et al. (2003).

The Osage C-1 core (Fig. 1) has 15 m of discontinuous core (slabbed) of the 'basal' Arbuckle between 1035-1051m. Based on lithostratigraphic correlation and similar stratigraphic and petrographic findings, this section is interpreted to represent part of the basal Gasconade Dolomite (Fig. 2 and 4, Appendix 5) and is partially or wholly composed of the Gunter Sandstone Member. The interval consists of cyclical wavy, skeletal-peloidal wackestone, burrowed wackestone-mudstone, sandy tidal flat laminites, sandy, cryptalgal stromatolites, and dolomitic sandstones. Sandstones are composed of sub-rounded, medium grained (0.06-0.15 mm), medium sorted quartz grains with intergranular porosity up to 5% (visually estimated). Vuggy zones were primarily observed in burrowed mudstones-wackestones. Rounded, pseudomorphs of gypsum nodules(<1-2cm in size) were observed in the core (Fig. 6f). Additionally, possible 'chicken wire' textures are observed in core. The base of cycles is eroded with pebbly zones, highly stylotized zones, increased sand content and coarser crystalline planar-nonplanar dolomite.

The Meisner MH 2 (Fig. 1) has 34m continuous core (slabbed) of the 'upper' Arbuckle between 1902-1936m. It is composed of meter-scale shoaling upward cycles that are interpreted to be part of the Cotter/Powell Dolomite (Fig. 2 and 4, Appendix 6). Thick (>2 m) sections of subtidal, burrowed wackestones, mottled-laminated mudstones, cryptmicrobial laminites, pelletal-skeletal packstones and cross-bedded oolitic grainstones were observed. Soft sediment deformation is observed close to the interfaces of sand-rich mudstones and clay-rich, laminated mudstones (Fig. 6g). Intercrystalline porosity is typical in all facies observed with fracture, vuggy, and moldic secondary porosity of up to 5% (visually estimated). The most porous zones are in burrowed mudstones-wackestones and contain vugs that measure 1 cm in the longest dimension.

The Wichert 1 core (Fig. 1) has 24 m continuous core (slabbed) between 2883-2907m in the 'upper' Arbuckle. It is composed of meter-scale shoaling upward cycles that are interpreted to be part of the Cotter/Powell Dolomite (Fig. 2 and 4, Appendix 7). Thick (>2 m) sections of subtidal, burrowed wackestones and laminated mudstones are overlain by oolitic grainstones and

packstones. In cycles observed near the top of the cored interval, crinkly laminated or cryptmicrobial laminates are overlain by subtidal, organic-rich mudstone facies (Fig. 6h, and 6i). Intercrystalline porosity is found in all facies with mainly fracture secondary porosity. Very little vuggy and moldic porosity was observed in this section. Fine-grained (<0.03 mm) quartz and silt-rich laminations are present in mudstone facies.

Petrography

Replacement Dolomite Petrography

Most of the dolomite observed in the Arbuckle Group is replacive dolomite of pre-existing limestone. Figure 7 displays the representative lithologic fabrics and dolomitic textures associated with replacement dolomite. Distinguishing between very fine to medium crystalline planar and medium to coarse crystalline planar and nonplanar replacement dolomite was important in identifying relationships between lithologic facies, dolomitic texture and cathodoluminescent (CL) patterns. Distinctive CL compositional zonation is present in replacement dolomite and dolomite cements in the study area. Typically, CL zonation consists of a dull, mottled to non-CL center followed by one to five zones alternating between non-CL and dull to moderately bright CL.

Replacement dolomite in subtidal, burrowed mudstones is typically unimodal, very fine to fine crystalline (<0.01 mm) planar-s dolomite with intercrystalline porosity. Very fine to fine crystalline, planar-s replacement dolomite in subtidal mudstones generally display dull to moderately bright CL and lack compositional zonation. Replacement dolomite in subtidal to intertidal burrowed-skeletal wackestones and pelletal-skeletal packstones display polymodal, fine to medium crystalline (<0.01-0.05 mm) planar-e to planar-s with mimically replaced allochems. Differences are observed in dolomite textures where allochems are present. Fine to medium crystalline (0.01-0.05 mm) planar-e textures filling allochem ghosts typically display open,

moldic or fenestral porosity. CL microstratigraphy in fine to medium crystalline (<0.01-0.05 mm), planar-e to planar-s replacement dolomites typically consists of either dull to moderately bright CL with no compositional zonation or dull to moderately bright CL displaying up to 2-3 compositional zones. When zonation is present, it generally consists of the following sequence of compositional zones: Z1) dull or moderately bright, mottled CL core, Z2) less bright, variable thickness, non-CL zone, and Z3) bright, CL outer rim. Replacement dolomite observed in dolomitic sandstones and replacing cryptmicrobial stromatolites are comprised of medium (0.01-0.03 mm) planar-s dolomite crystals and display similar CL patterns to those described above (Fig. 7c).

Medium to coarse crystalline (0.03-0.7mm), planar to nonplanar replacement dolomite is observed in pelletal-skeletal packstones, dolomitic sandstones and cryptmicrobial stromatolites. CL microstratigraphy in medium to coarse crystalline (0.03-0.7 mm), planar to nonplanar dolomite display up to four to five zones including: Z1) dull to moderately bright, mottled CL core, Z2) dull to bright, mottled CL zone (potentially partially dissolved), Z3) dull to non-CL zone, and Z4) dull to moderately bright, CL outer zone and Z5) dull to non-CL, thicker outer zone.

Open Space Filling Cements

Dolomite cements occupying open pore spaces (fractures, vugs, molds) display the most complex CL zonation (up to six compositional zones) (Fig. 8). Void-filling dolomite cements are typically coarse (0.05-10 mm) crystalline, nonplanar dolomite cement (saddle dolomite). These cements are observed in a range of facies throughout all cores studied. Infrequently, quartz cement was observed lining large vugs and as fracture fill cement. Quartz cement displays no CL response. CL microstratigraphy of coarse (0.05-10 mm), saddle dolomite displays two to six compositional zones (Fig. 9 and 10). Compositional zonation patterns typically consist of: Z1) dull to non-CL

mottled CL core, Z2) mottled to non-CL, outer CL core, Z3) dull, thick CL zone, Z4) dull, CL zone, Z5) lighter, dull CL outer zone. Irregular CL banding and the most complex CL pattern was observed in medium to coarse crystalline (0.05-10 mm), saddle dolomite in the Gasconade Dolomite and Gunter Sandstone Member respectively. This compositional zonation pattern consists of: Z1) dull to moderately bright, mottled CL core, Z2) non-CL to dull, homogenous, CL outer core, Z3) banded, dull to moderately bright, CL zone (Z4 truncates Z3 and displays irregular banding), Z4) banded, bright to moderately bright, CL zone, Z5) bright, non-banded CL zone, and Z6) dull to non-CL zone. Both the Shads 4 and Osage C-1 cores display irregular banding in coarse, saddle dolomite (Fig. 9c-9f).

Fluid Inclusion Microthermometry

Dolomite Cements

Primary, two phase inclusions (liquid and vapor) observed in coarse (0.05-10mm) saddle dolomite were measured for vapor homogenization temperature (T_h), ice melting temperature (T_m) and eutectic temperature (T_e) when possible. Inclusions ranged in size from 3-10 μm with a mean size of 6 μm. Smaller inclusions were observed and measured; however, the confidence of the measurements for these inclusions varies due to poor optical resolutions. No petroleum inclusions were observed. The inclusions contain ~2-10% vapor volume at room temperature (21°C) and vapor bubble movement at room temperature was common. One hundred and twenty-four fluid inclusions were analyzed for T_h and T_m temperature values, out of which both T_h and T_m measurements were obtained on sixty-nine fluid inclusions. Fluid inclusion assemblages were plotted for each core using salinities calculated from measured T_m values and equations from Bodnar (1992) for dolomite cements (Fig. 11, Table 2).

In the Shads 4 core, T_h of primary fluid inclusions in dolomite range from 90.80 to 142.55°C with an average of 115.01°C and median of 115.60°C (Fig. 11 and Table 2). T_m values range from -

25.90° to -17.85°C with an average of -21.49°C and median of -22.00°C. Salinities ranged from 20.9 to 26.1 wt. % NaCl equivalent. Five T_e measurements were collected from five different assemblages and ranged from -40.8 to -40.0°C.

In the Osage C-1 core, T_h values of primary fluid inclusions in dolomite range from 95.90° to 154.30°C with an average of 122.49°C and median of 116.67°C (Fig. 11 and Table 2). T_m values range from -27.30° to -19.05°C with an average of -22.74°C and median of -22.71°C. Salinities ranged from 21.7 to 27.0 wt. % NaCl equivalent. Four T_e measurements were collected from four different assemblages and ranged from -44.3 to -34.5°C.

In the Meisner MH 2 core, T_h values of primary fluid inclusions in dolomite range from 89.98° to 122.80°C with an average of 109.33°C and median of 110.79°C (Fig. 11 and Table 2). T_m values range from -35.70° to -17.50°C with an average of -24.93°C and median of -23.45°C. Salinities ranged from 20.6 to 32.6 wt. % NaCl equivalent. One T_e measurement of -40.2°C was made. Two data points from Meisner MH 2 (1915m) are considerably more saline (~33 wt. % NaCl equivalent) despite displaying cooler temperatures (~100°C). These fluid inclusions were among the smallest (<3 μm) measured.

In the Wichert 1 core, T_h values of primary fluid inclusions in dolomite range from 115.40° to 131.10°C with an average of 123.66°C and median of 123.73°C (Fig. 11 and Table 2). T_m values range from -22.55° to -18.57°C with an average of -21.15°C and median of -21.60°C. Salinities ranged from 21.4 to 24.0 wt. % NaCl equivalent.

Nearly 80% of all 124 T_h measurements fall within the range of 90° to 130°C with 100% of all measurements between 90° to 155°C. Nearly 70% of all 69 T_m measurements fall within -25° to -20°C with 100% between -35°to -15°C. Inclusions plot as two distinct populations: a lower temperature (89°C to 128°C) with moderate salinity (20 to 27 wt. % NaCl equivalent) and higher temperature (128°C to 154°C) with moderate salinity (20 to 27 wt. % NaCl equivalent).

Isotope Geochemistry

Fine crystalline planar replacement dolomites generally displayed $\delta^{13}C$ and $\delta^{18}O$ values in equilibrium with early Ordovician seawater or (and/or modified seawater (Veizer et al., 1999), ranging from $\delta^{13}C$ -2.5 to -1.6‰ VPDB and $\delta^{18}O$ -9 to -5‰ VPDB. Fine crystalline, planar replacement dolomites display $\delta^{13}C$ values ranging from -3.84 to -0.63 ‰ VPDB and $\delta^{18}O$ values ranging from -7.92 to -3.08‰ VPDB (Fig. 12 and Table 3). Medium to coarse crystalline planar-nonplanar replacement dolomite display $\delta^{13}C$ values ranging from -2.72 to -1.61‰ VPDB and $\delta^{18}O$ values ranging from -7.94 to -6.17‰ VPDB. Values for $\delta^{13}C$ or $\delta^{18}O$ in either fine planar or medium to coarse planar-nonplanar replacement dolomites displayed no significant trends in the vertical section when compared with depth.

Dolomite cements display $\delta^{13}C$ values ranging from -3.49 to -0.98 ‰ VPDB and $\delta^{18}O$ values ranging from -9.46 to -4.25‰ VPDB (Fig. 12 and Table 3). Values of $\delta^{13}C$ or $\delta^{18}O$ in dolomite cements displayed no significant trends in the vertical section when compared with depth.

Fine crystalline planar replacement dolomite display values of $^{87}Sr/^{86}Sr$ ranging from 0.70946 to 0.70986. $^{87}Sr/^{86}Sr$ values measured for medium to coarse crystalline planar-nonplanar replacement dolomite ranged from 0.70947 to 0.70972 Values of $^{87}Sr/^{86}Sr$ for coarse crystalline saddle dolomite cement ranged from 0.70969 to 0.71029.

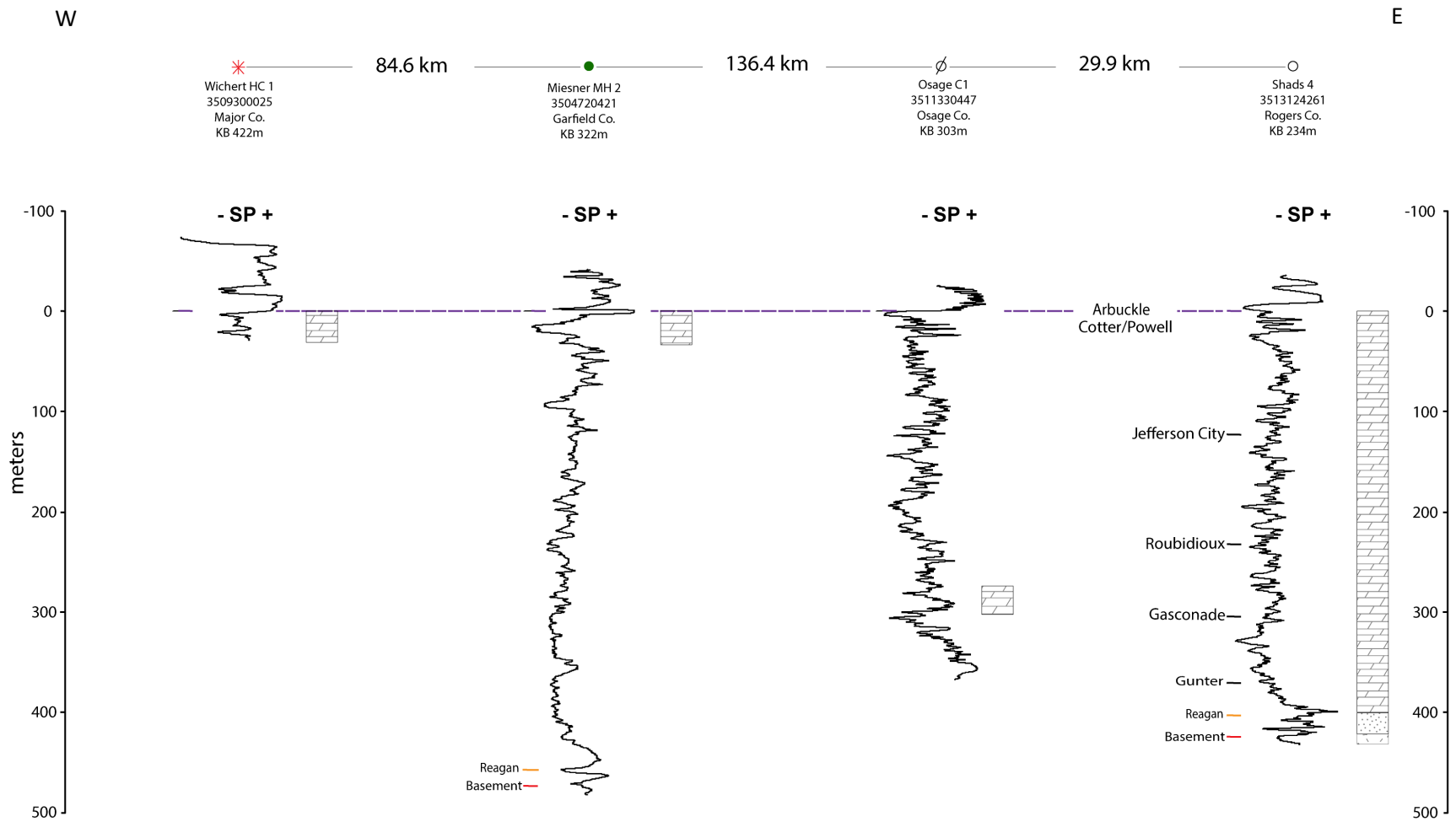

Figure 4. *Lithostratigraphic correlation of cored intervals*. The Osage C-1 core sampled the basal Gasconade Formation (Gunter Sandstone Member), and both the Meisner MH 2 and Wichert 1 cores sampled the Cotter-Powell and/or Jefferson City Dolomite.

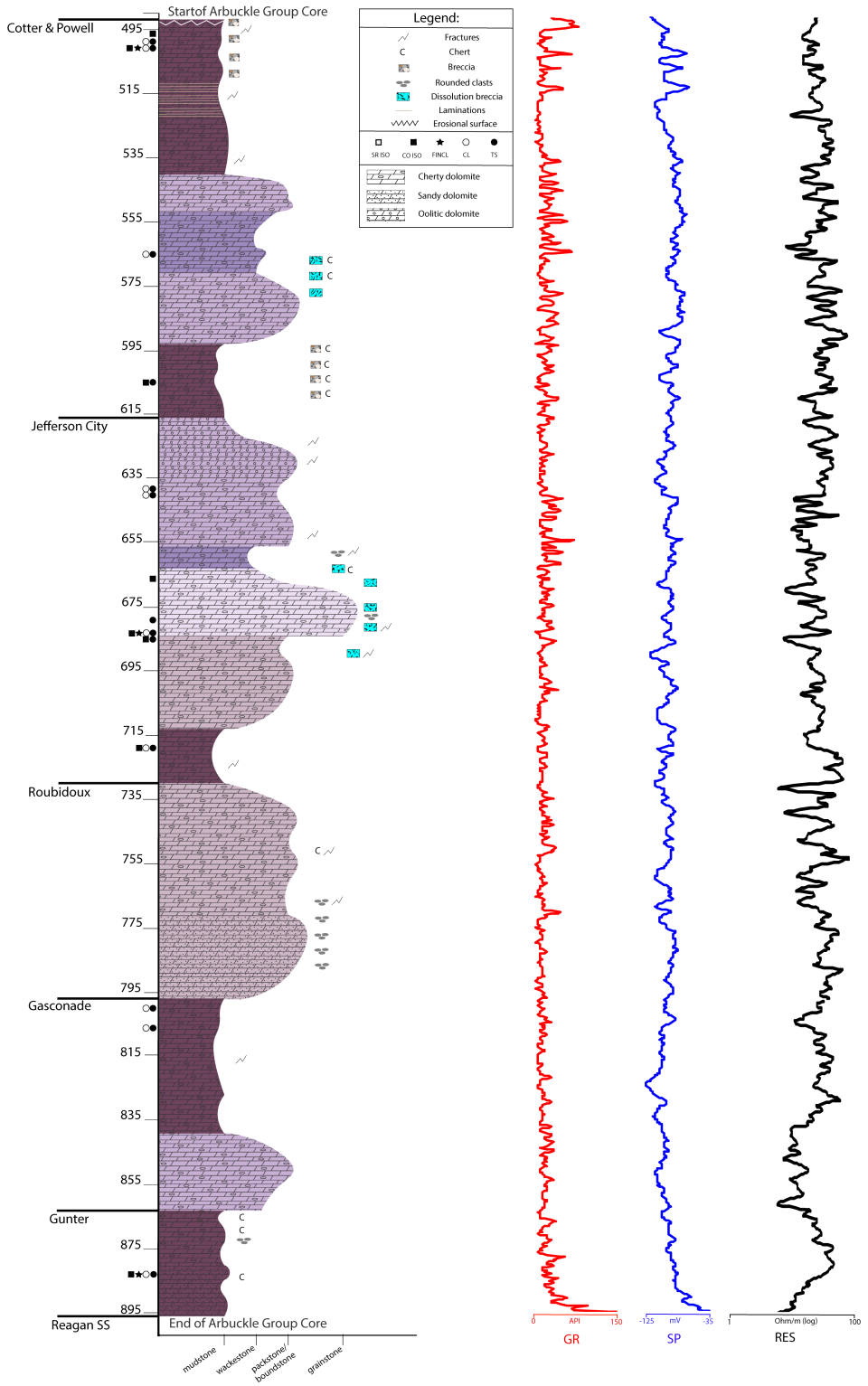

Figure 5. *Shads 4 core diagram with electric logs*. Shads 4 has 422m of continuous core of the complete Arbuckle section for the interval of 493m to 895m (modified after Derby, 1991).

Figure 6. *Lithology of core and representative core features*. a) Vuggy zone (lined with dolomite) within laminites in the Gasconade Dolomite (Shads 4). b) Isolated, solution-enlarged vugs are open-filled with saddle dolomite cement crystals that are as large as 7 cm in the longest dimension in the Jefferson City Dolomite (Shads 4). c) Oolitic (grainstone) chert (Shads 4). d) Suspended, rounded, oolitic (packstone-grainstone) chert within a mudstone in the Jefferson City Dolomite (Shads 4). e) Cross-section of a large stromatolite in the Cotter-Powell Dolomite (Shads 4). f) Polygonal-to-globular shaped, centimeter-sized pseudomorphs of gypsum nodules. Wispy, organic seams (mechanically compacted) are observed draping gypsum nodules (Osage C1; 1cm scale). g) Soft sediment deformation is observed close to the interfaces of sand-rich mudstones and clay-rich, laminated mudstones (Meisner MH 2). h) Stromatolitic 'bump' within cryptmicrobial laminites (left); homogenous, organic-rich mudstone (right; Wichert 1). i) Homogenous, organic-rich mudstone with intermittent laminations (Wichert 1; 5cm scale).

Figure 7. *Petrography of replacement dolomite*. a) Very fine-fine crystalline, planar-s dolomite replacing laminated mudstone with occasional, very thin, silty laminations (Shads 4; PPL). b) Very fine to fine crystalline, planar-s dolomite replacing burrowed, pelletal mudstone (Meisner MH 2; PPL); vertical burrow with a slightly coarser crystalline planar dolomite (left) moldic porosity at the top of the vertical burrow (right). c) Micritized peloids-pellets (left), very fine-medium crystalline planar-s to planar-e polymodal dolomite replacing peloidal-pelletal-skeletal wackestone (Meisner MH 2; PPL); pyro-bitumen-filled, sub-horizontal fracture (right). d) Very fine to fine crystalline, planar dolomite replacing cryptmicrobial, 'crinkly' laminites (Meisner MH 2; PPL); organic matter and fine silts that were trapped in microbial mats (left). e) Very fine to fine crystalline, planar dolomite replacing organic-rich, laminated mudstones (Wichert 1; XL). f) Fine crystalline planar dolomite replacing homogenous mudstone (Meisner MH 2; XL). g) Medium to coarse crystalline, planar-e dolomite replacing peloidal, vuggy mudstone (Shads 4; PPL); open vugs can be nearly 1mm in size (left). h) Fine-medium crystalline, planar-nonplanar polymodal dolomite replacing a fenestral carbonate (Shads 4; XL); micritized peloids (left); open pore space in fenestrae (right). Note: PPL (plane polarized light), XL (cross polarized light).

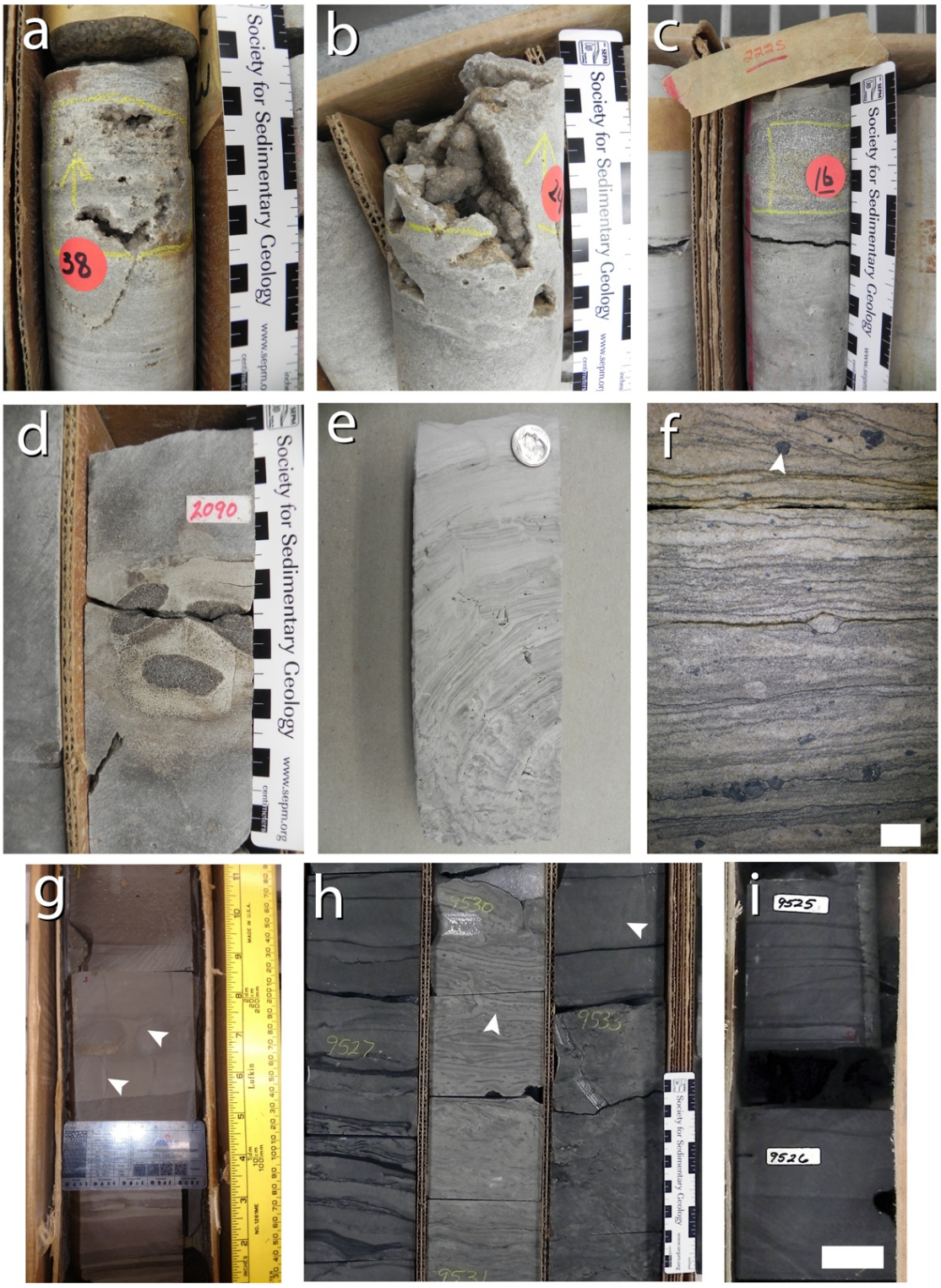

Figure 6. *Lithology of core and representative core features*.

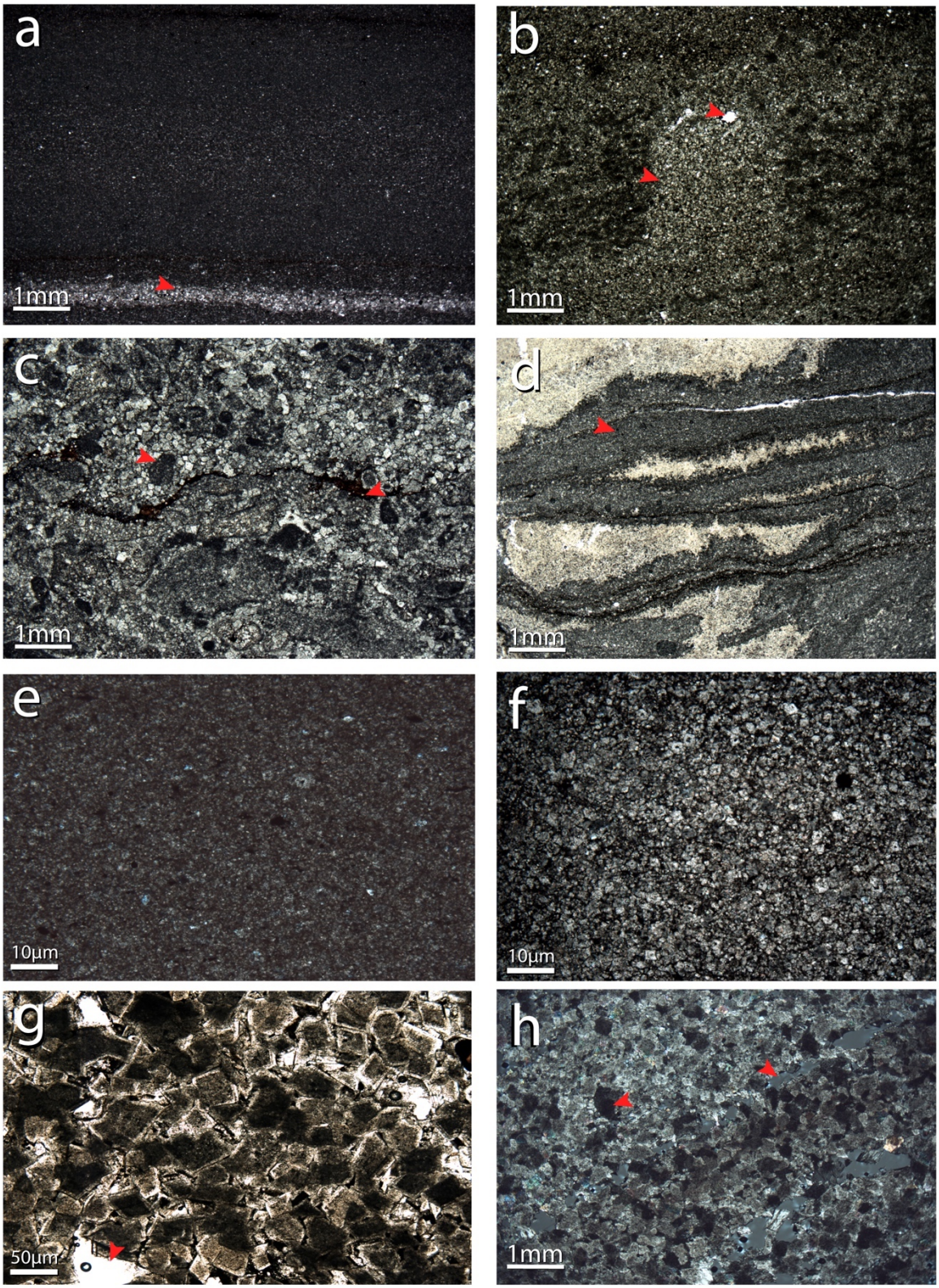

Figure 7. *Petrography of replacement dolomite*.

Figure 8. *Petrography of dolomite cements.* a) Coarse crystalline, saddle dolomite cement filling a solution-enlarged fracture and vug within a laminated mudstone (Meisner MH 2; XL). b) Coarse crystalline, saddle dolomite cement filling a vertical fracture that terminates at a high relief stylolite (Meisner MH 2; PPL). c) Coarse crystalline, saddle dolomite cement lining a large (>2cm in longest dimension), solution-enlarged vug (Shads 4; PPL). Open pore space exists within the vug. d) Medium-coarse crystalline, saddle dolomite cement filling an isolated vug within a homogenous mudstone (Meisner MH 2; PPL). e) Coarse crystalline, saddle dolomite cement (left) with fine sediment filling, forming a geopetal structure (Meisner MH 2; PPL). This photomicrograph is rotated 90° counterclockwise from the vertical position of the field of view. f) Coarse crystalline, saddle dolomite cement filling collapsed skeletal material (left; Wichert 1 XL); fine crystalline, replacive dolomite (right). g) Coarse crystalline, saddle dolomite cement (SD) filling a large vug (>4cm). The vug is lined with quartz (Q) and medium crystalline, saddle dolomite cement. Fine-medium crystalline, dolomite replaced (RD) the host rock adjacent to the vug (Shads 4; PPL). h) XL photomicrograph of the same field as (g). Note: PPL (plane polarized light), XL (cross polarized light).

Figure 9. *CL photomicrograph representative of the range of the observed CL microstratigraphy*. a) Coarse crystalline, saddle dolomite cement filling a vug in a skeletal wackestone (Wichert 1; PPL). b) CL photomicrograph of the same field as (a). c) Coarse crystalline, saddle dolomite cement lining a large (>2cm) vug in the 'basal' Arbuckle (Shads 4; PPL). d) CL photomicrograph of the same field as (c). e) Coarse crystalline, saddle dolomite cement filling a vug in the 'basal' Arbuckle (Osage C1; PPL). f) CL photomicrograph of the same field as (e). g) Coarse crystalline, saddle dolomite cement filling an isolated vug (Shads 4; PPL). h) CL photomicrograph of the same field as (g).

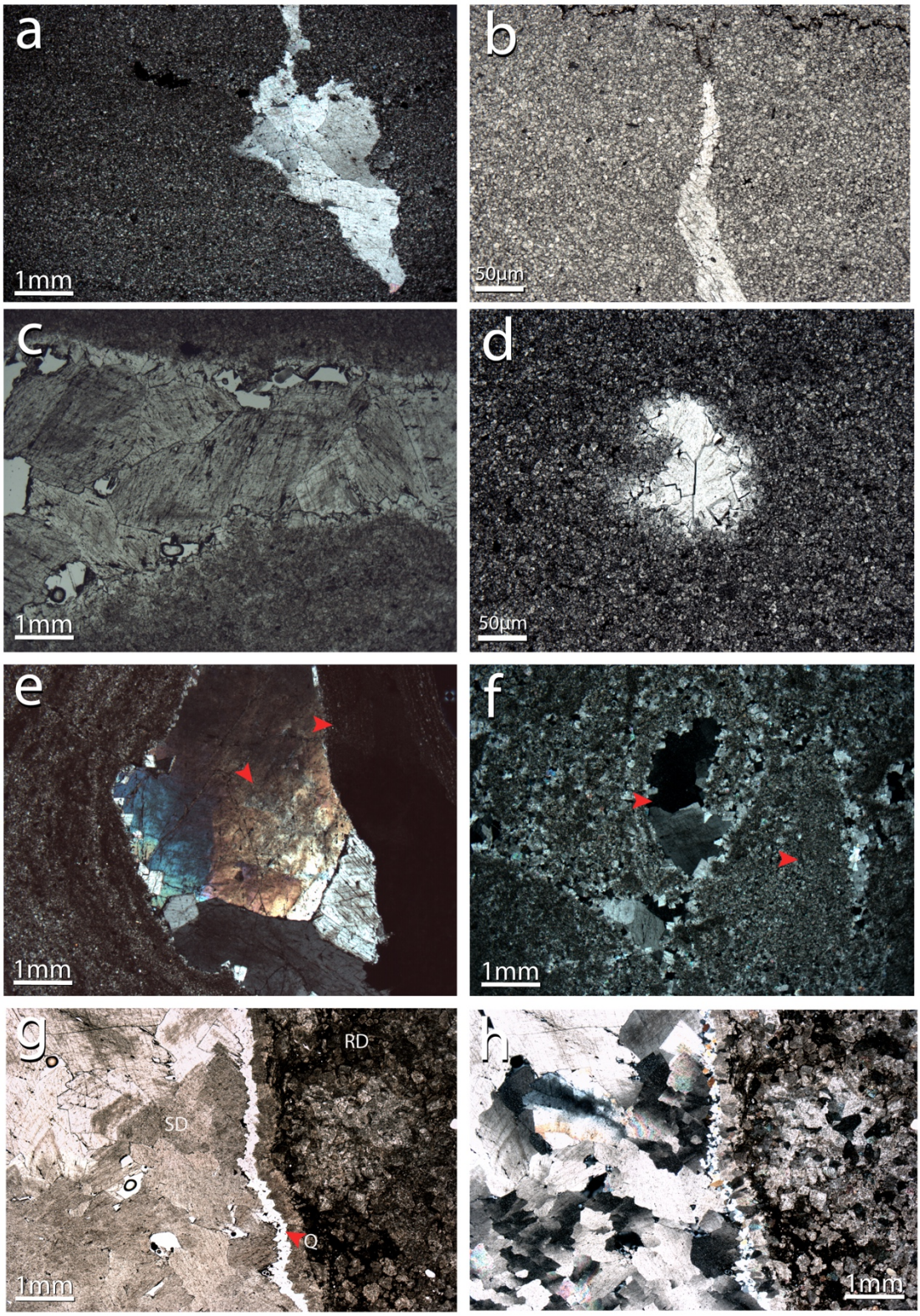

Figure 8. *Petrography of dolomite cements*.

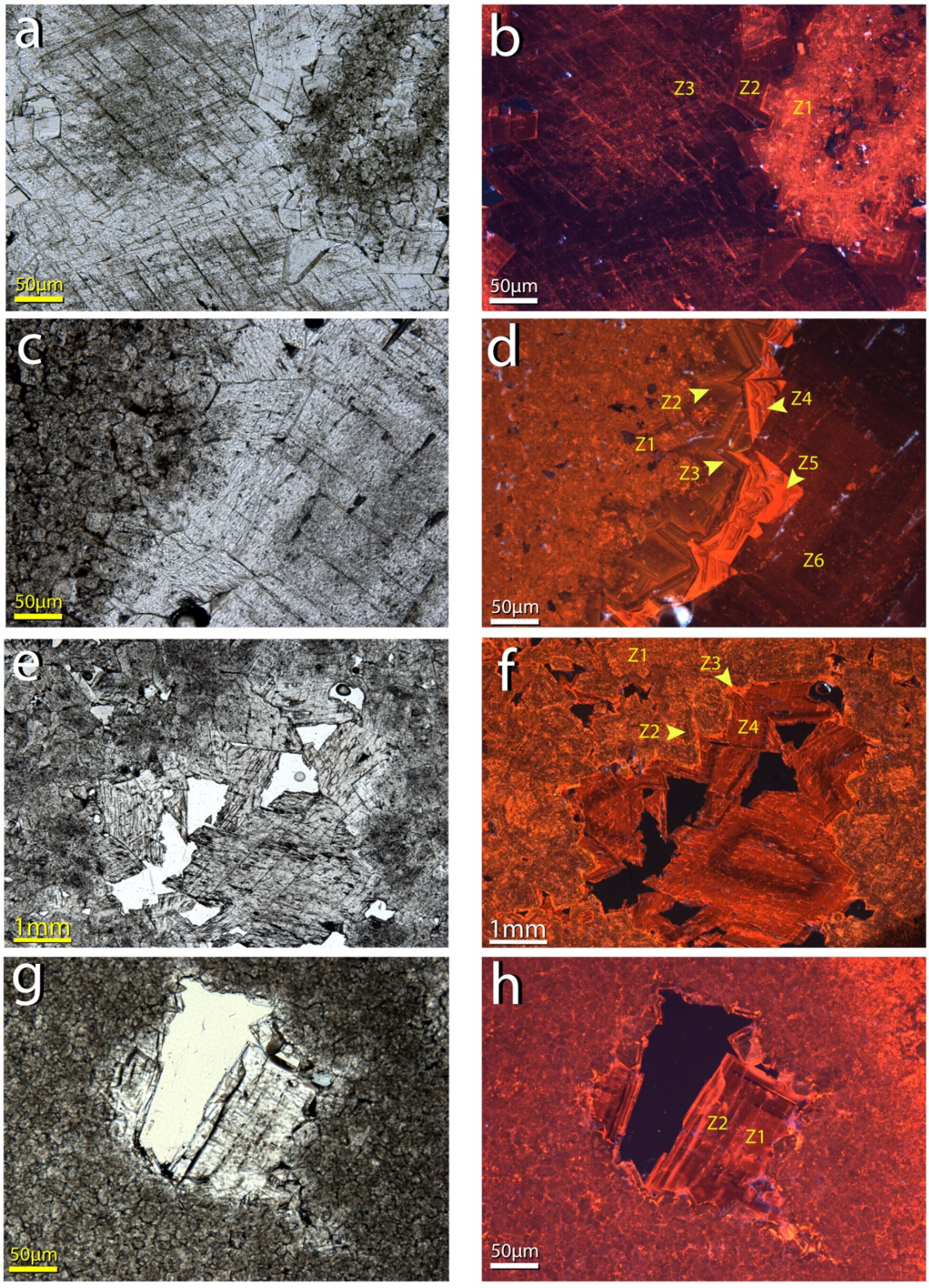

Figure 9. *CL photomicrograph representative of the range of the observed CL microstratigraphy.*

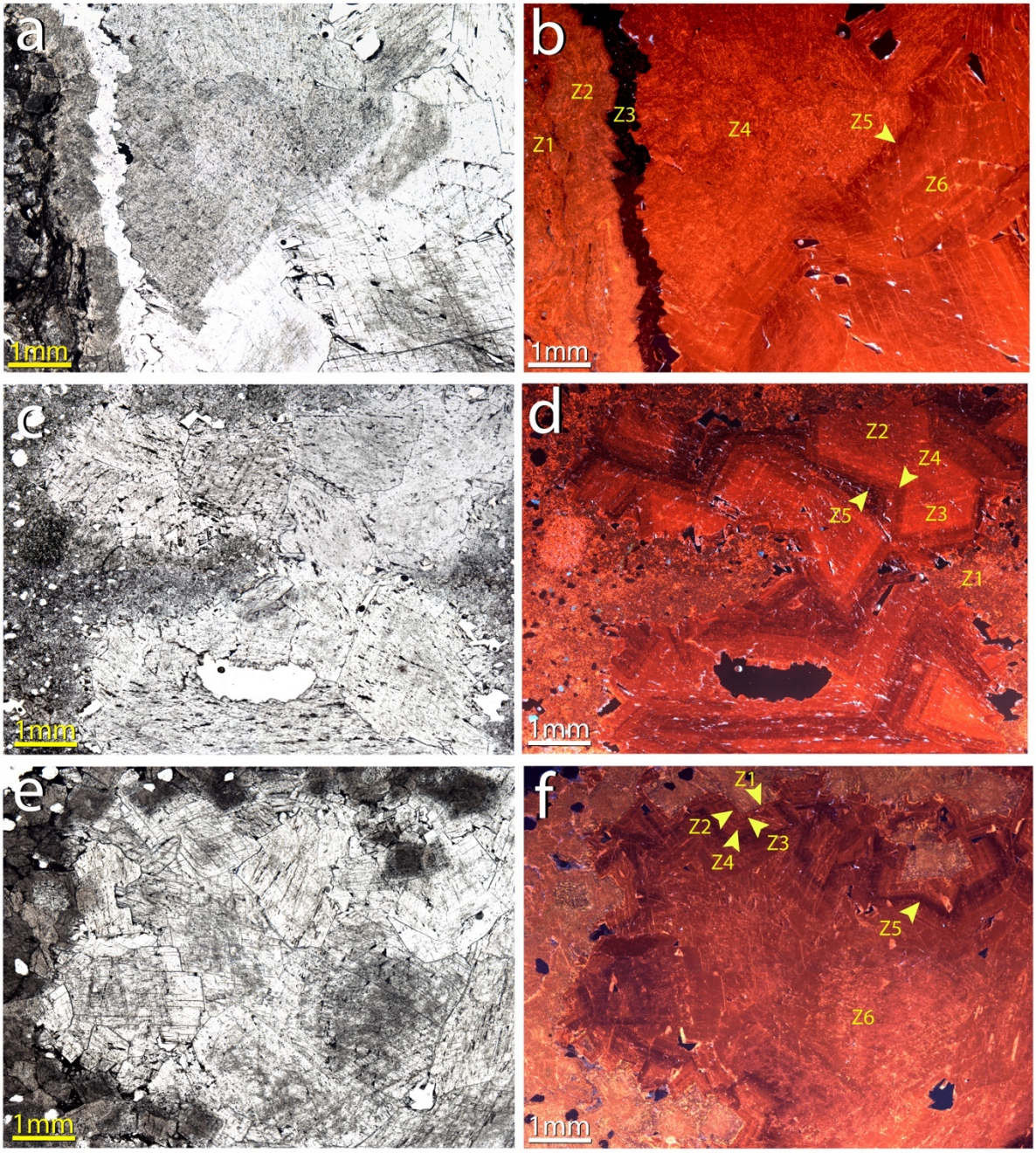

Figure 10. *CL composite photomicrographs of Jefferson City and Gasconade Dolomites*. a) Coarse crystalline, saddle dolomite cement in the 'upper' Jefferson City Dolomite (Shads 4; PPL). b) CL photomicrograph of the same field as (a). c) Coarse crystalline, saddle dolomite cement in the 'lower' Jefferson City Dolomite (Shads 4; PPL). d) CL photomicrograph of the same field as (c). e) Coarse crystalline, saddle dolomite cement and sub-rounded quartz grains in the 'lower' Gasconade Dolomite (Osage C1; PPL). f) CL photomicrograph of the same field as (e).

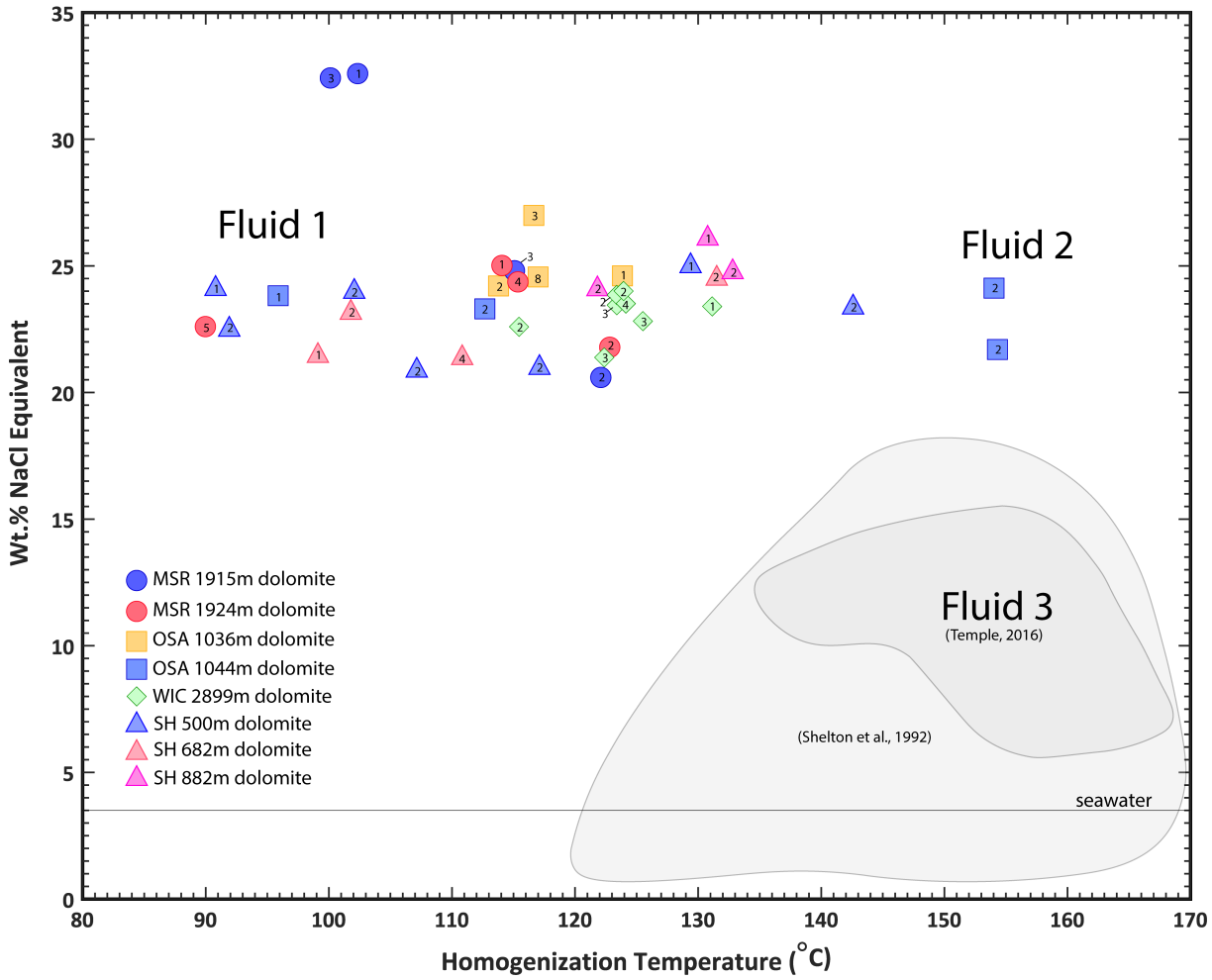

Figure 11. *Plot of fluid inclusion assemblage' s salinities vs. T_h values for inclusions observed*. Fluid inclusions plot as two distinct populations: a lower temperature and moderate salinity fluid, and a higher temperature and moderate salinity fluid. There are two data points (Meisner MH 2) that plot as an anomalously lower temperature and higher salinity fluid. Fluid 3 is plotted as observed by Shelton et al. (1992) and Temple (2016).

Sample ID	Location	Assemblage	Mineral	T_h°C	T_m°C	Calculated Salinity (wt. % eq. NaCl)
SH 500m	Rogers Co., OK	Assemblage 1	Dolomite	102.1	-22.4	24.0
		Assemblage 2	Dolomite	90.8	-22.6	24.1
		Assemblage 3	Dolomite	107.2	-17.9	20.9
		Assemblage 4	Dolomite	91.9	-20.2	22.5
		Assemblage 5	Dolomite	129.4	-24.1	25.0
		Assemblage 6	Dolomite	142.6	-21.6	23.4
		Assemblage 7	Dolomite	117.2	-18.0	21.0
SH 682m	Rogers Co., OK	Assemblage 1	Dolomite	131.5	-23.2	24.5
		Assemblage 2	Dolomite	110.8	-18.7	21.4
		Assemblage 3	Dolomite	99.1	-18.7	21.5
		Assemblage 4	Dolomite	101.8	-21.3	23.2
SH 882m	Rogers Co., OK	Assemblage 1	Dolomite	121.8	-22.6	24.1
		Assemblage 2	Dolomite	130.8	-25.9	26.1
		Assemblage 3	Dolomite	132.8	-23.7	24.8
		Assemblage 4	Dolomite	115.6	-	-
OSA 1036m	Osage Co., OK	Assemblage 1	Dolomite	117.0	-23.3	24.5
		Assemblage 2	Dolomite	113.8	-22.8	24.2
		Assemblage 3	Dolomite	114.3	-	-
		Assemblage 4	Dolomite	116.7	-27.3	27.0
		Assemblage 5	Dolomite	123.8	-23.4	24.6
OSA 1044m	Osage Co., OK	Assemblage 1	Dolomite	154.0	-22.6	24.1
		Assemblage 2	Dolomite	112.7	-21.4	23.3
		Assemblage 3	Dolomite	154.3	-19.1	21.7
		Assemblage 4	Dolomite	95.9	-22.1	23.8
MSR 1915m	Garfield Co., OK	Assemblage 1	Dolomite	107.5	-	-
		Assemblage 2	Dolomite	100.2	-35.5	32.4
		Assemblage 3	Dolomite	104.0	-	-
		Assemblage 4	Dolomite	102.3	-35.7	32.6
		Assemblage 5	Dolomite	122.1	-17.5	20.6
		Assemblage 6	Dolomite	115.1	-23.8	24.8
MSR 1924m	Garfield Co., OK	Assemblage 1	Dolomite	115.3	-23.1	24.4
		Assemblage 2	Dolomite	122.8	-19.5	21.8
		Assemblage 3	Dolomite	114.1	-24.1	25.0
		Assemblage 4	Dolomite	90.0	-20.3	22.6
WIC 2899m	Major Co., OK	Assemblage 1	Dolomite	123.4	-22.2	23.8
		Assemblage 2	Dolomite	123.5	-21.7	23.5
		Assemblage 3	Dolomite	131.1	-21.5	23.4
		Assemblage 4	Dolomite	115.4	-20.4	22.6
		Assemblage 5	Dolomite	124.1	-21.8	23.5
		Assemblage 6	Dolomite	125.5	-20.6	22.8
		Assemblage 7	Dolomite	124.0	-22.6	24.0
		Assemblage 8	Dolomite	122.4	-18.6	21.4

Table 2. *Fluid inclusion assemblage data for saddle dolomite cements in the study area.*

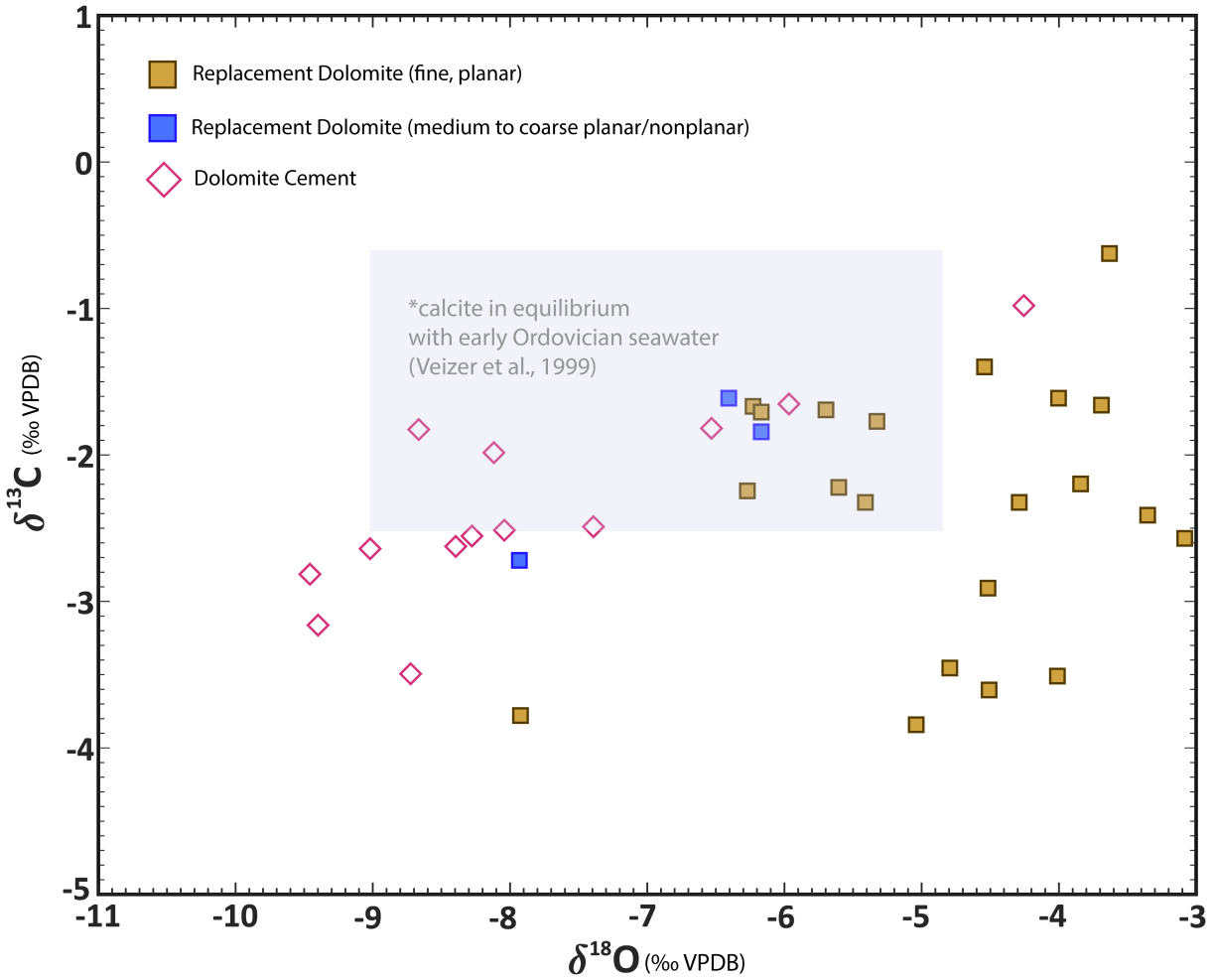

Figure 12. *Stable isotopes values of $\delta^{13}C$ and $\delta^{18}O$.* Stable isotopes values of $\delta^{13}C$ and $\delta^{18}O$ (per mil VPDB) for fine planar replacement dolomite, medium to coarse planar-nonplanar replacement dolomite, and dolomite cement from the study area. Early Ordovician seawater values obtained from Veizer et al. (1999).

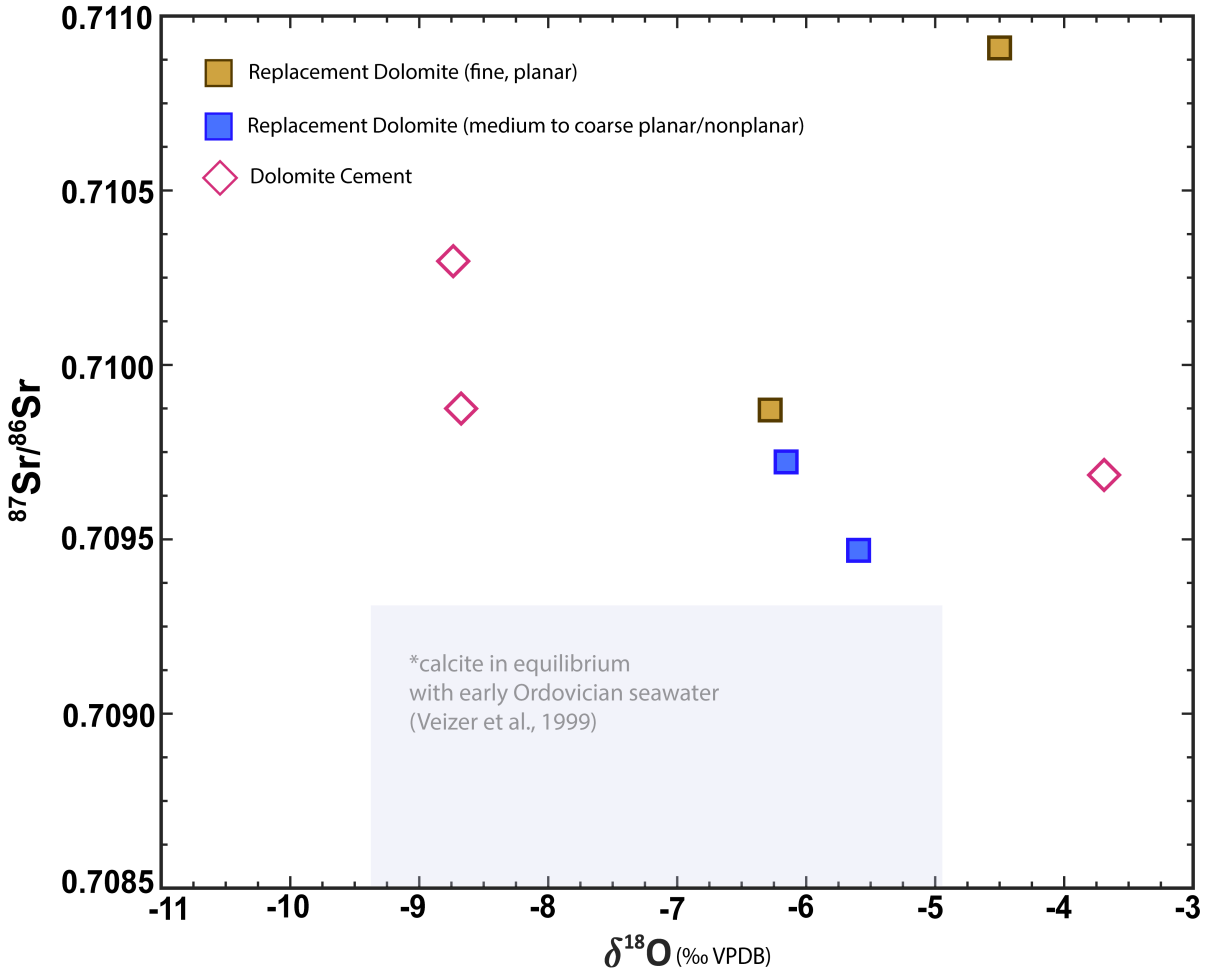

Figure 13. *Stable isotopes values of $^{87}Sr/^{86}Sr$ versus $\delta^{18}O$.* Stable isotopes values of $^{87}Sr/^{86}Sr$ versus $\delta^{18}O$ (per mil VPDB) for fine planar replacement dolomite, medium to coarse planar-nonplanar replacement dolomite, and dolomite cement from the study area. Early Ordovician seawater values obtained from Veizer et al. (1999).

Sample ID	Mineral	$\delta^{13}C$	$\delta^{18}O$	$^{87}Sr/^{86}Sr$
SH 496m	Replacement Dolomite	-2.2	-3.8	
SH 500m	Replacement Dolomite	-3.5	-4.8	
SH 604m	Replacement Dolomite	-2.3	-5.4	
SH 669m	Replacement Dolomite	-3.8	-7.9	
SH 682m	Replacement Dolomite	-1.7	-6.2	0.70987
SH 682m	Replacement Dolomite	-2.2	-6.3	
SH 718m	Replacement Dolomite	-2.2	-5.6	0.70947
SH 882m	Replacement Dolomite	-3.8	-5	
SH 718m	Dolomite Cement	-2.8	-9.5	
SH 500m	Dolomite Cement	-2.6	-9	
SH 604m	Dolomite Cement	-3.2	-9.4	
SH 682m	Dolomite Cement	-2.6	-8.4	
SH 682m	Dolomite Cement	-2.5	-8	
SH 882m	Dolomite Cement	-3.5	-8.7	0.7103
OSA 1036m	Replacement Dolomite	-1.7	-6.2	0.70972
OSA 1039m	Replacement Dolomite	-2.7	-7.9	
OSA 1039m	Replacement Dolomite	-1.8	-6.2	
OSA 1044m	Replacement Dolomite	-1.6	-6.4	
OSA 1036m	Dolomite Cement	-1.8	-8.7	0.70988
MSR 1903m	Replacement Dolomite	-3.6	-4.5	0.71091
MSR 1907m	Replacement Dolomite	-1.8	-5.3	
MSR 1914m	Replacement Dolomite	-2.3	-4.3	
MSR 1915m	Replacement Dolomite	-1.6	-4	
MSR 1919m	Replacement Dolomite	-0.6	-3.6	
MSR 1923m	Replacement Dolomite	-1.4	-4.5	
MSR 1924m	Replacement Dolomite	-1.7	-3.7	
MSR 1929m	Replacement Dolomite	-2.4	-3.4	
MSR 1915m	Dolomite Cement	-2	-8.1	
MSR 1919m	Dolomite Cement	-1	-4.3	
MSR 1924m	Dolomite Cement	-2.5	-7.4	0.70969
MSR 1929m	Dolomite Cement	-2.6	-8.3	
WIC 2883m	Replacement Dolomite	-3.5	-4	
WIC 2899m	Replacement Dolomite	-1.7	-5.7	
WIC 2904m	Replacement Dolomite	-2.6	-3.1	
WIC 2905m	Replacement Dolomite	-2.9	-4.5	
WIC 2899m	Dolomite Cement	-1.8	-6.5	
WIC 2899m	Dolomite Cement	-1.7	-6	

Table 3. *Stable isotope data for replacement dolomite and dolomite cements in the study area*.

CHAPTER V

DISCUSSION

Sedimentation and Early Diagenesis

During the early Ordovician, widespread limestone deposition occurred throughout the Midcontinent on a broad, shallow, carbonate platform to low-gradient ramp interrupted by increased siliciclastic (intrabasinal) input with punctuated, regional to sub-regional unconformities indicative of repeated meter-scale sea level changes (He at al., 1997; Overstreet et al., 2003; Fritz et al., 2012; Temple, 2016).

The range of lithofacies and cycle stacking patterns observed in the Arbuckle Group of northeastern and north-central Oklahoma are consistent with previous works on the Midcontinent (He et al., 1997, Overstreet et al., 2003; Franseen, 2004; Temple, 2016; King, 2013; Fritz et al., 2012). Thick (>2 m) subtidal to intertidal cyclical facies appear to have dominated the Jefferson City, Cotter, and Powell Dolomite in the westernmost portion of the study area (Wichert 1, Meisner MH 2) with thinner (0.5 to >2m) subtidal to supratidal cyclical facies in the Jefferson City, Cotter, and Powell Dolomite on the Cherokee Platform (Osage C-1, Shads 4). The Gasconade Dolomite and Roubidoux Formation are also interpreted to be largely deposited in

subtidal to intertidal environments but with variable siliciclastic input throughout the section on both the Anadarko Shelf and Cherokee Platform. The idealized cycles described by Overstreet et al., 2003 provided a reference for the cores examined in this study. Type I cycles observed in the study area consists of thinner (< 2m) packages of burrowed-mottled, mudstone-wackestones overlain by pelletal-oolitic packstones and grainstones and capped by intertidal laminites and microbial stromatolites (*i.e.* Overstreet et al., 2003). Type II cycles observed in the study area consists of thicker (> 2m), subtidal dominated cycle bases of homogenous to burrowed mudstone-wackestones overlain by intertidal cryptmicrobial and mechanical laminites (*i.e.* Overstreet et al., 2003).

Although dolomitization tends to be fabric destructive, original (limestone) depositional fabrics in the Arbuckle are largely preserved in the study area (*e.g.* Moñtanez, 1992). Early diagenetic dolomitization mechanisms are thought to differ in supratidal/uppermost intertidal sections and subtidal facies (*e.g.* Moñtanez, 1992; He et al., 1997; Overstreet et al., 2003; Fritz et al., 2012; Temple, 2016). Early replacement dolomite of the Arbuckle Group was likely formed syndepositionally within tidal flats under relatively low-temperature and low-pressure conditions (*e.g.* Moñtanez, 1992; Sibley and Gregg, 1987). Supratidal facies consist of mainly cryptmicrobial laminites and are replaced by a range of very fine to medium crystalline planar to nonplanar replacement dolomite. Intertidal facies consist of pelletal-intraclastic wackestones and cryptmicrobial laminites and are also replaced by a range of very fine to medium crystalline, planar to nonplanar replacement dolomite. Supratidal and the uppermost intertidal facies may have been completely or partially dolomitized syndepositionally and affected by subaerial exposure thus contributing to the creation of secondary porosity such as vugs and molds observed in the facies (*e.g.* Moñtanez, 1992; Fritz et al., 2012). Dolomitization throughout these sections of the Arbuckle likely occurred by an evaporative pumping mechanism (Temple, 2016). Seawater saturating the sediment, moves up due to the capillary effect during evaporation from the surface

causing an increase in gypsum precipitation leading to a loss in Ca^{2+} and an increase in Mg/Ca ratios (Fig. 14). Ultimately, groundwater becomes increasingly concentrated in Mg resulting in dolomitization (Hsu and Siegenthaler, 1970). Subtidal facies consist of mainly homogenous to burrowed-mottled mudstones and wavy, peloidal wackestones and are largely replaced by very fine to fine crystalline, planar replacement dolomites. Dolomitization of subtidal sediments may have occurred due to refluxing brines (Adams and Rhodes, 1960) that were formed in the overlying supratidal and uppermost intertidal sections that seeped down slowly into the original limestone (Fig. 14). The degree of dolomitization of subtidal facies during early diagenesis likely varied in the section and may have ranged from completely undolomitized to completely dolomitized. Modern analogs for such dolomitization mechanisms are observed in the Persian Gulf sabkha environments and are associated with deposits of gypsum and halite (Patterson and Kinsman, 1982; McKenzie et al., 1980). Evidence for evaporites are commonly observed in Lower Ordovician sections on the Midcontinent (Overstreet et al., 2003).

Fine crystalline planar replacement dolomites display $\delta^{13}C$ and $\delta^{18}O$ values in equilibrium with early Ordovician seawater and evaporated seawater ranging from $\delta^{13}C$ -2.5 to -1.6‰ VPDB and $\delta^{18}O$ -9 to -5‰ VPDB (Fig. 12; Veizer, 1999). This is consistent with the interpretation that much of the original limestone was dolomitized early and retained the carbon and oxygen isotopic signature of the original diagenetic environment (Fig. 15). Replacement dolomites that have retained the carbon and oxygen isotopic signature of early Ordovician seawater typically display dull, mottled to non-CL cores (Moñtanez, 1992). Fine crystalline planar replacement dolomite that plots as less negative ('heavier') oxygen isotopes values and outside of the range of early Ordovician seawater can be explained by dolomitization occurring in seawater modified by evaporation. After initial stabilization in modified seawater, continued stabilization may have occurred during karst developments in fresh or mixed water aquifers (*e.g.* Moñtanez and Read, 1992). Fine planar replacement dolomite with $\delta^{13}C$ values between -4.0 to 0‰ VPDB and $\delta^{18}O$

values between -5.0 to -3‰ VPDB may indicate increased microbial sulfate reduction or oxidation of organic matter (Hudson, 1977; Swart, 2015).

Pelletal-oolitic packstones and grainstones are typically replaced by chert but also display fine crystalline replacement dolomite as pellets and ooids that were selectively replaced with replacement dolomite as isopachous rims (*e.g.* Moñtanez, 1992). The timing of chert replacement and early dolomitization looks to be consistent with a paragenetic pattern that places chert replacement prior to replacement dolomite (*i.e.* Temple, 2016). The evidence for this is the preservation of internal textures of ooids in oolitic cherts. If dolomitization occurred prior to chert replacement, the internal fabric of the grains would have been destroyed by dolomitization. Additionally, eroded oolitic chert clasts observed in subtidal facies may not have withstood transport if chert replacement did not occur prior to early dolomitization.

Late Diagenesis

Medium to coarse crystalline planar-nonplanar replacement dolomite is interpreted to be partially or completely recrystallized early diagenetic replacement dolomite by basinal fluids during late diagenesis (*e.g.* Sibley and Gregg, 1987; Gregg and Shelton, 1990). Gregg and Sibley (1984) concluded these textures can indicate dolomite growth under epigenetic (dolomitization at elevated temperatures) conditions above 50°C. Additionally, polymodal textures were more commonly observed in these recrystallized replacement dolomites further indicating partial recrystallization of early, fine planar dolomite into medium to coarse crystalline nonplanar dolomite. CL of medium to coarse crystalline, planar-nonplanar replacement dolomite display dull, mottled to non-CL cores but also display CL banding in outer zones similar to CL microstratigraphy in void-filling, coarse crystalline saddle dolomite cements. This suggests that early replacement dolomite CL cores remained partially intact and basinal fluids precipitated

syntaxial cement overgrowths onto these cores that are contemporaneous with saddle dolomite cements.

The range for limestone in equilibrium with early Ordovician seawater is broad and may overlap substantially with fine planar replacement dolomites and saddle dolomite cements; however, medium to coarse crystalline planar to nonplanar replacement (recrystallized) dolomite typically displays more negative $\delta^{18}O$ values than fine planar replacement dolomites. This is expected if this rock was partially or completely reset (with respect to carbon and oxygen isotopic compositions) by warm, saline basinal fluids.

Void-filling saddle dolomite cements in secondary porosity, including vugs, molds and fractures, represents the latest stage of dolomitization in the Arbuckle Group. Void-filling saddle dolomite cements is thought to indicate precipitation at temperatures above 60°C in burial settings and/or from warm, saline basinal fluids ascending upward through strata (Radke and Mathis, 1980; Gregg and Sibley, 1984). CL zonation observed in void-filling dolomite cements result from changing chemical composition (Fe^{2+} and Mn^{2+}) of the precipitating fluids indicating geochemically evolving fluids moving through the reservoir (Gregg and Shelton, 2012; Gregg et al., 2012; Temple, 2016).

CL microstratigraphy of coarse crystalline saddle dolomite cements is correlative across the section with some slight variances of the complexity of depending on location and stratigraphic position. Irregular CL banding in the Shads 4 and Osage C-1 cores may be indicative of at least partial dissolution of Z1 and Z3. Similarity exists between the irregular CL banding in the study area and southern Missouri (Gregg and Hagni, 1987). Dissolution of dull to non-CL replacement dolomite cores may be indicative of early diagenetic interaction with fresh or mixed water aquifer systems (*e.g.* Moñtanez and Read, 1992). Alternatively, dissolution occurred in the deep burial setting with the passing of multiple, geochemically distinct, warm, saline fluids. One or more of

the fluids being a metalliferous brine that caused dissolution in dolomite as critical 'poisoning' levels produced complex faceting (Gregg and Hagni, 1987). The latter explanation is more plausible given the proximity to MVT base metal deposits of northeastern Oklahoma and southeastern Missouri.

Although overlapping with early Ordovician seawater, carbon and oxygen isotope geochemistry of dolomite cements largely display more negative ('lighter') $\delta^{18}O$ values than early diagenetic textures and medium to coarse planar to nonplanar replacement dolomites. This is consistent with the interpretation that these cements precipitated in equilibrium with the warm, saline basinal (hydrothermal) fluids (Fig. 16; Fritz et al., 2012). Portions of Arbuckle strata that were in close proximity to or within a fault zone with enhanced fracture networks may have been preferential fluid flow conduits for hydrothermal (fluids at least 5-10°C warmer than surrounding host rock) fluids that interacted with continental basement (Fig. 16).

Fluid inclusion microthermometry provides the strongest evidence for the precipitation of saddle dolomite cements by warm, saline basinal fluid(s) having a temperature and salinity range 89°C to 154°C and 20 to 27 wt. % NaCl equivalent, respectively (Fig. 11; Table 2). Shelton et al. (1992) and Temple (2016) interpreted their fluid inclusion data to indicate either mixing of two end-member saline fluids, shown as Fluids 1 and 2 in Figure 11, or a cooling trend in one saline fluid. The range of homogenization temperatures measured for this study are interpreted similarly. A third component fluid, Fluid 3 (Fig. 11) was not observed in this study area and may be fluid originating in the Ozark region and did not migrate westward into this study area.

Strontium isotope data for the study area is problematic. A majority (> 85%) of the $^{87}Sr/^{86}Sr$ ratios values indicate a continental basement or basement-derived sedimentary rock signature ($^{87}Sr/^{86}Sr$ ratios > 0.7095) and is higher than that would be expected for carbonates in equilibrium with early Ordovician seawater (Veizer et al., 1999). Banner et al. (1990) and Shelton et al. (2009)

predict a covariation of oxygen and strontium isotopes that express a mixing trend between early Ordovician seawater and water that has equilibrated with continental basement. However, this mixing trend is not observed in oxygen and strontium isotope values in in this study by Temple (2016). The only explanation that can be offered for these observations is that all of the dolomite studied were reset with respect to basinal fluids that derived their $^{87}Sr/^{86}Sr$ composition from continental basement or sedimentary rocks derived from continental basement.

Origin, Timing and Evolution of Late Diagenetic Fluid Flow

Previous research suggests basin fluid flow events correspond on the Midcontinent of North America correspond with Ouachita (Alleghenian coeval) orogeny tectonism during the Late Pennsylvanian and Permian Periods (Bethke and Marshak, 1990; Viets and Leach, 1990; Shelton et al. 1992; Appold and Garven, 1999). Basinal brines are thought to have migrated northward from the Arkoma and/or the Anadarko basins through a gravity (topographical) driven fluid flow system (Appold and Garven, 1999). The gravity-driven basin fluid flow model described by Appold and Garven (1999) explains a mechanism in which deep basinal brines migrate towards the basin margin under a hydraulic gradient established by the Alleghenian/Ouachita orogeny. As the brine fluid migrated through the Arbuckle, the excess heat was conducted to adjacent strata partially explaining an anomalous thermal history of organic sediments in the Arkoma Basin (Bethke and Marshak, 1990).

Musgrove and Banner (1993) observed recent groundwater mixing of geochemically distinct fluids that affect the Ozark region today. If today's mixing trend is indicative of the presence of past mixing trends, this may explain why the missing, less saline third end member fluid (Fluid 3, Fig. 11) is found within or in closer proximity to the Ozark Plateau aquifer where fluids are more meteoric in origin compared to sources from the Western Interior Plains aquifer system and Southwestern Interior Plains aquifer system (Mugrove and Banner; 1993). Additionally,

Musgrove and Banner (1993) also described a very saline groundwater (evaporated sea water source made up of Na-Ca-Cl) originating from the Anadarko Basin that are present in the western portion of the study area today. They believe that this is a remnant Paleozoic age fluid. An Anadarko basin derived basinal fluid may aid in explaining the anomalous calculated salinities (~33 wt. % NaCl equivalent) along the Nemaha Fault Zone. The timing of the development of the Anadarko Basin (late Mississippian through Pennsylvanian) compared to the expected timing of brine migration (Pennsylvanian-Permian) overlap substantially (Perry, 1989; Bethke and Marshak, 1990). This may suggest a mechanism for basin fluid flow in the Anadarko Basin that transported a warm, very saline (>30 wt. % NaCl equivalent), fluid through the Arbuckle Group. An alternative interpretation for the missing Fluid 3 end member in the study area is the distance from the Reelfoot Rift fluid source in southeastern Arkansas which may have been the source of less saline, high temperature fluids throughout the Paleozoic (Keller et al., 2000; Shelton et al. 1992).

Based on fluid inclusion data, these basinal fluids may have been sourced from the Arkoma and/or the Anadarko basins. Warm, saline fluids (89°C to 154°C and 20 to 27 wt. % NaCl equivalent) migrated through the Arbuckle Group (preferentially) driven by a gravity-driven fluid flow system during and/or after the Alleghenian/Ouachita orogeny. Eutectic temperatures measured further indicate that these fluids were not simple NaCl brines but complex saline brines consisting of Ca, Mg, Na chlorides and sulfates.

Petroleum fluid inclusions are rare in the Arbuckle Group. Neither Shelton et al. (1992) or Temple (2016) observed petroleum fluid inclusions in southern Missouri or northeastern Oklahoma. King (2013) observed primary, pseudosecondary, and secondary petroleum fluid inclusions in the Arbuckle in saddle dolomite cements in southern Kansas postulating the migration of petroleum during or during and after saddle dolomite precipitation. Although the

evidence is not widespread, the explanation of King (2013) may offer insight into the timing of petroleum migration in the Arbuckle Group.

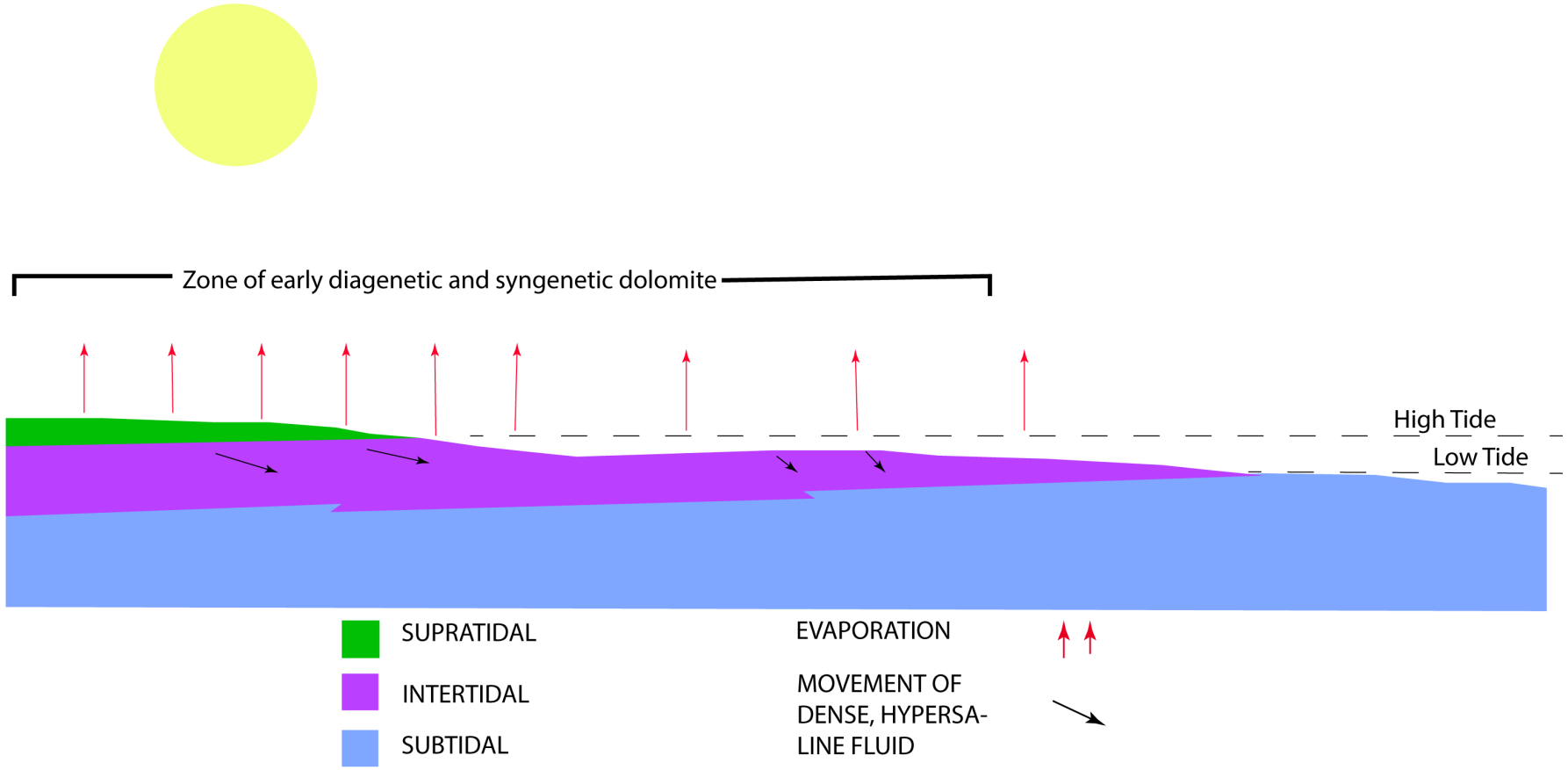

Figure 14. *Conceptual early diagenetic model*. Extensive, early dolomitization occurred during early diagenesis by two main mechanisms: evaporative pumping and refluxing brines (after Fritz et al., 2012).

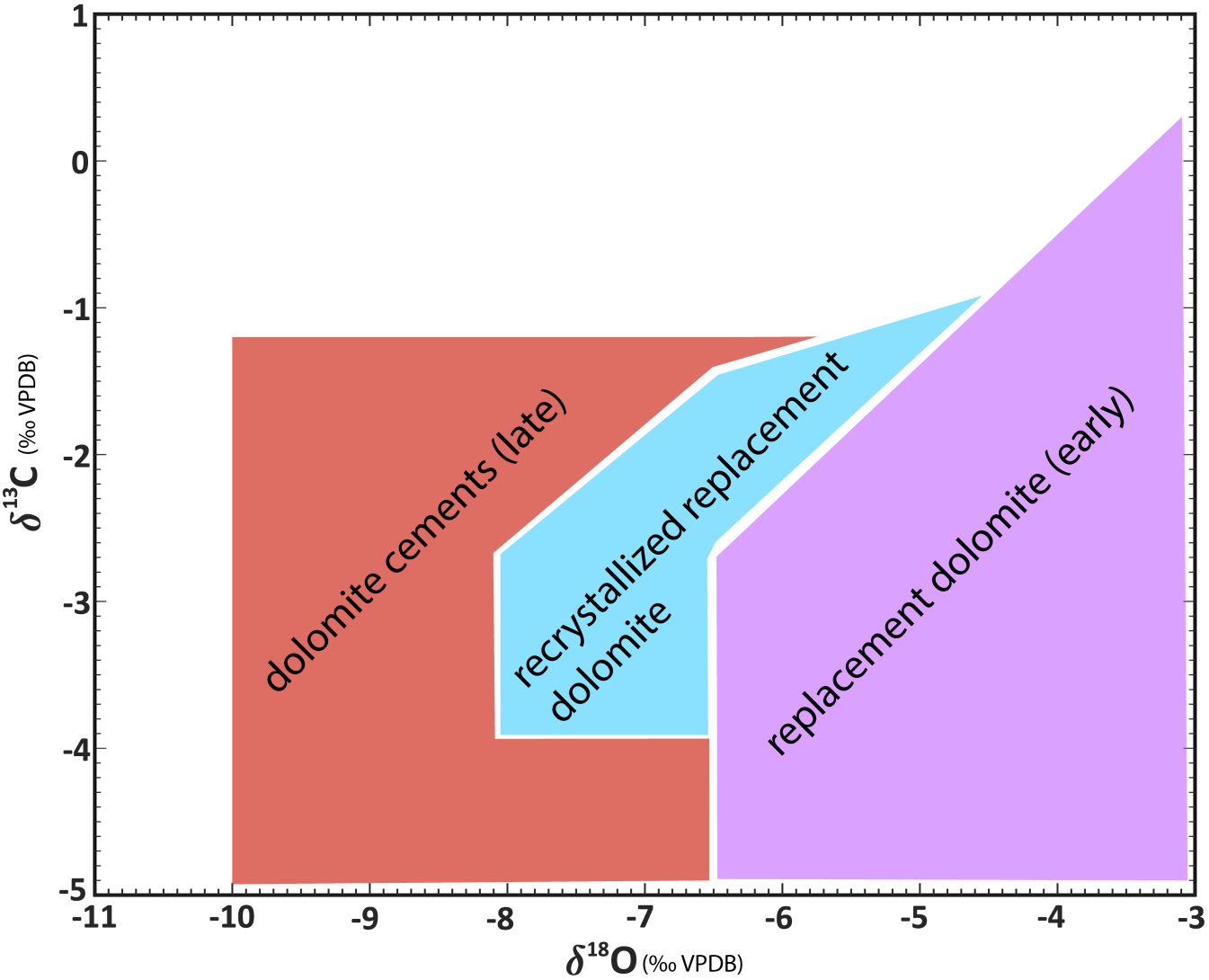

Figure 15. *Interpretation of stable carbon and oxygen isotopes*.

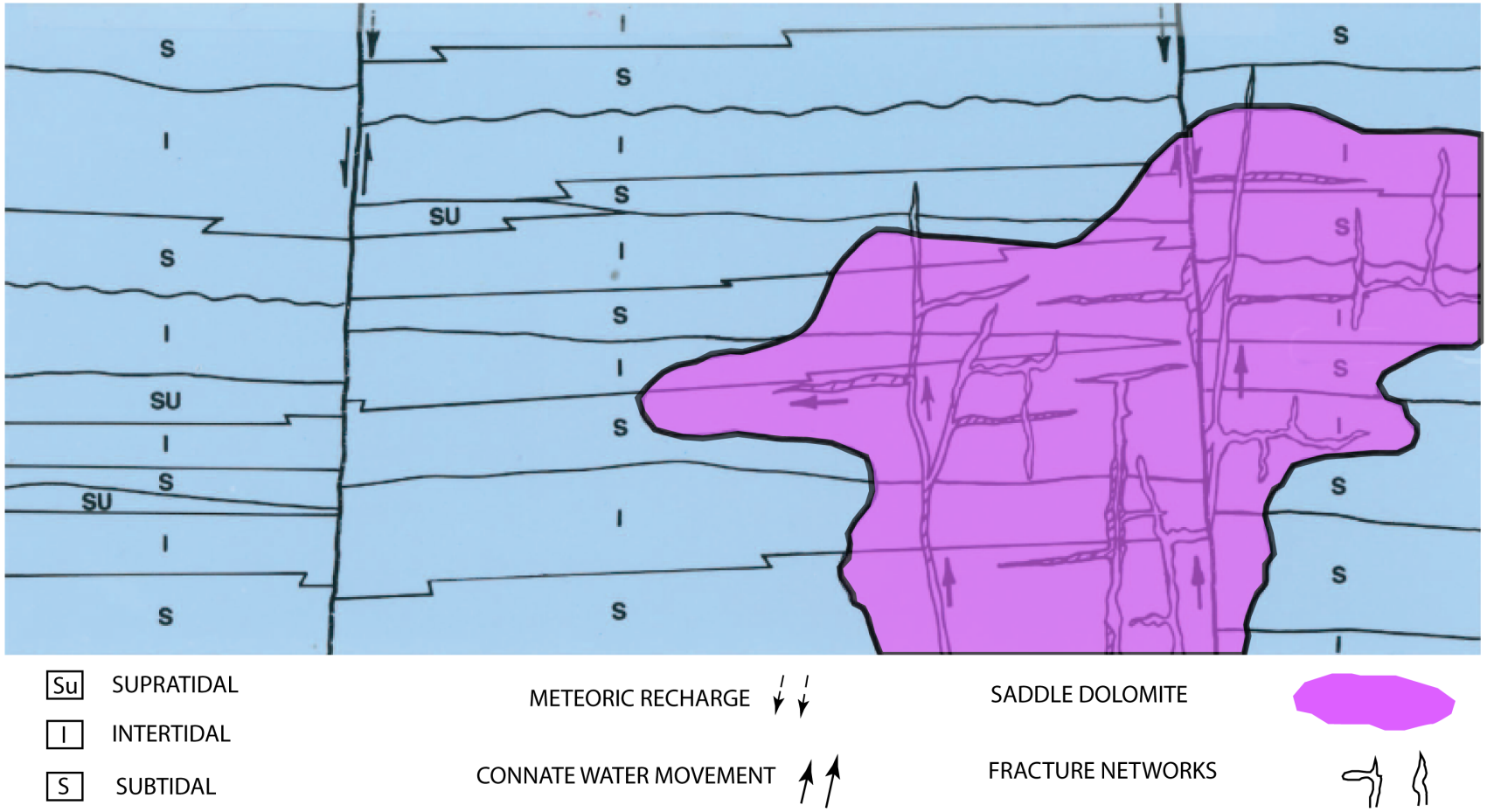

Figure 16. *Conceptual dolomitization model for late diagenesis (saddle dolomite)*. Saddle dolomite cements precipitated from hydrothermal fluids (after Fritz et al., 2012).

CHAPTER VI

CONCLUSIONS

Multiple stages of dolomitization affected Arbuckle Group carbonates of the Midcontinent. Extensive dolomitization was initially constrained to selective facies within shallow platform, meter-scale, shoaling upward cycles. During early diagenesis, fine planar replacement dolomite formed syndepositionally in supratidal facies and both supratidal and the uppermost intertidal facies were dolomitized by evaporative pumping mechanisms. Portions of intertidal and subtidal facies were dolomitized by refluxing brines that were formed in the overlying sections.

During burial, basinal fluids and groundwater (in aquifer hosted systems) preferentially migrated within the established flow conduits further dissolving (in the case of fresh or mixed water systems) or recrystallizing early replacement dolomite. Fracture networks created during and/or after the Alleghenian/Ouachita orogeny and uplifting during the Laramide orogeny (associated deep-seated fault movement) interrupted once discrete flow units promoting vertical migration of hydrothermal fluids from continental basement.

Most of the dolomite in the Arbuckle in the study area was at least partially recrystallized during late diagenesis by warm, saline basinal fluids. Warm saline brines (89°C to 154°C and 20 to 27 wt. % NaCl equivalent) are responsible for precipitation of late dolomite cements. The fluid may have cooled as it migrated through the Arbuckle from the Arkoma and/or Anadarko basins as it

ascended through the section. Hydrothermal fluids (>90°C) that precipitated saddle dolomite cements migrated through deep-seated faults and associated fracture networks that were likely conduits for fluid flow.

The data presented in this study are consistent with the prevailing hypotheses of (a) Arbuckle Group carbonates in northeastern and north-central Oklahoma were modified by both early (seawater derived) fluids as wells as late diagenetic fluids and (b) migration of basinal fluids through a gravity driven flow system originating in the Arkoma and/or Anadarko basins.

REFERENCES

Adams J.E., and Rhodes, L., 1960, Dolomitization by seepage refluxion. Bull. Am. Assoc. Petrol. Geologists, v. 44, p. 1912-1920.

Ahr, W. M. 2008, Carbonate Reservoir Rock Properties, in Geology of Carbonate Reservoirs: The Identification, Description, and Characterization of Hydrocarbon Reservoirs in Carbonate Rocks, John Wiley & Sons, Inc., Hoboken, NJ, USA. doi: 10.1002/9780470370650.

Appold, M.S., Garven, G., 1999, The hydrology of ore formation in the Southeast Missouri district: numerical models of topography-driven fluid flow during the Ouachita orogeny: Economic Geology, v. 94, p. 913-936.

Banner, J.L., and Hanson, G.N., 1990, Calculation of simultaneous isotopic and trace element variations during water-rock interaction with applications to carbonate diagenesis: Geochimica et Cosmochimica Acta, v. 54, p. 3123-3137.

Bartram, J. G., Imbt, W. C., and Shea, E. F., 1950, Oil and gas in Arbuckle and Ellenburger Formations, Mid-Continent region: American Association Petroleum Geologists Bulletin, v. 34, p. 682-700.

Bethke, C. M., and Marshak, S., 1990, Brine migrations across North America - the plate tectonics of groundwater. Annual Review of Earth and Planetary Sciences, 18, 287-315.

Bizzell, K. R., 2017, Structural Characterization of the Galena Township Fault Zone: Woodward, Woods, and Major Counties, Oklahoma, University of Tulsa, Unpublished Master's Thesis, 136, p. 1-116.

Bodnar, R.J., 1992, Revised equation and table for determining the freezing point depression of H2O-NaCl solutions: Geochimica et Cosmochimica Acta, v. 57, p. 683-684.

Campbell, J., A., Grasmick, M., K., 1991, Oil and Gas in Arbuckle Group Reservoirs in Oklahoma: An NRIS Perspective: Oklahoma Geological Survey Circular 92: Late Cambrian-Ordovician Geology of the Southern Midcontinent, 1989 Symposium, p. 189-202.

Chenoweth, P. A., 1968, Early Paleozoic (Arbuckle) overlap, southern Mid-Continent, United States: American Association Petroleum Geologists Bulletin, v. 52, p. 1670-1688.

Christenson, S., Osborn, N.I., Neel, C.R., Faith, J.R., Blome, C.D., Puckette, James, and Pantea, M.P., 2011, Hydrogeology and simulation of groundwater flow in the Arbuckle-Simpson aquifer, south-central Oklahoma: U.S. Geological Survey Scientific Investigations Report 2011–5029, 104 p.

Denison, R.E., 1981, Basement Rocks in Northeastern Oklahoma, Oklahoma Geological Survey Circular, v. 84, 88, p. 1-81.

Derby, J.R., Hinch, H. H., and Repetski, J. R., 1991, Lithology, stratigraphy, and age of the Arbuckle Group in the Amoco SHADS No. 4, a continuous core from grassroots into basement, Rogers County, Oklahoma: Oklahoma Geological Survey, Special Publication 91-3, p. 69-82.

Derby, J.R., Raine, R.J., Runkel, A.C., and Smith, M.P., 2012, Paleogeography of the great American carbonate bank of Laurentia in the earliest Ordovician (early Tremadocian): The Stonehenge transgression, in J.R. Derby, R.D. Fritz, S.A. Longacre, W. A. Morgan, and C.A. Sternbach, eds., The great American carbonate bank: The geology and economic resources of the Cambrian – Ordovician Sauk megasequence of Laurentia: AAPG Memoir 98, p. 5-13.

Dillon, R. W., Anderson, N.L., Gregg, J.M., Cawlfield, J.D., 1998, Fire Clay Mining in Central Missouri: Geology and Mining Hazards: Highway Application of Engineering Geophysics with an Emphasis on Previously Mined Ground, Missouri Department of Transportation publishers, 11, p. 190-198.

Franseen, E.K., Byrnes, A.P., Cansler, J.R., SteinHauff, D.M., Carr, T.R., 2004, The Geology of Kansas Arbuckle Group, Kansas Geological Survey, Current Research in Earth Sciences, Bulletin 250 Part 2, 43, p. 1-41.

Fritz, R.D., P. Medlock, M.J. Kuykendall, and J.L. Wilson, 2012a, The geology of the Arbuckle Group in the mid-continent: Sequence stratigraphy, reservoir development, and the potential for hydrocarbon exploration, in J.R. Derby, R.D Fritz, S.A. Longacre, W.A. Morgan, and C.A. Sternbach eds., The Great American Carbonate Bank: The geology and economic resources of the Cambrian-Ordovician Sauk megasequence of Laurentia: AAPG Memoir 98, p.203-273.

Gao, G., Land, L.S., and Elmore, R.D., 1995, Multiple episodes of dolomitization in the Arbuckle Group, Arbuckle Mountains, south-central Oklahoma: Field, petrographic, and geochemical evidence: Journal of Sedimentary Research, v. A65, n. 2, p. 321-331.

Gatewood, L. E., 1978a, Some Oklahoma Arbuckle production and thoughts on fracturing: Shale Shaker, v. 29, p. 4-11.

Gatewood, L. E., 1978c, Stratigraphic trap possibilities in the Arbuckle Group general relationships: Shale Shaker, v. 28, p. 219-227.

Gentry, N.E., 2012, Carbonate-Hosted Sulfide Mineralization in the Southwest Davis Zinc Field, Southern Oklahoma, Oklahoma State University, Unpublished Master's Thesis, 62 p. 1-53.

Goldstein, R. H., and T. J. Reynolds, 1994, Systematics of fluid inclusions in diagenetic minerals: Society for Sedimentary Geology (SEPM) Short Course 31, 199 p.

Goldstein, R.H., 2001, Fluid inclusions in sedimentary and diagenetic systems. Lithos 55: 159-193.

Gregg, J. M., and Hagni, R. D., 1987, Irregular cathodoluminescent banding in late dolomite cements: evidence for complex faceting and metalliferous brines: Geological Society of America Bulletin, v. 98, p. 86-91.

Gregg, J.M., Laudon, P. R.2, Woody, R. E.2, and Shelton, K. L.2, 1993, Porosity evolution of the Bonneterre Dolomite (Cambrian) southeastern Missouri, U.S.A.: Sedimentology, v. 7, p. 1153-1169.

Gregg, J.M., Shelton, K. L., Johnson, A. W.2, Somerville, I. D., and Wright, W. R.2, 2001, Dolomitization of the Waulsortian Limestone (Lower Carboniferous) Irish Midlands: Sedimentology, v. 48, p. 745-766.

Gregg, J.M., and Shelton, K.L., 2012, Mississippi Valley-type mineralization and ore deposits in the Cambrian – Ordovician great American carbonate bank, in J. R. Derby, R. D. Fritz, S. A. Longacre, W. A. Morgan, and C. A. Sternbach, eds., The great American carbonate bank: The geology and economic resources of the Cambrian – Ordovician Sauk megasequence of Laurentia: AAPG Memoir 98, p. 163 – 186.

He, Z., Gregg, J.M., Shelton, K.L., and Palmer J.R., 1997, Sedimentary facies control of fluid flow and mineralization in Cambro-Ordovician strata, southern Missouri, in Moñtanez, I.P., Gregg, J.M., and Shelton, K.L., eds., Basin-wide diagenetic patterns: integrated petrological, geochemical, and hydrologic considerations: SEPM Special Publication no. 57, p. 81-99.

Hsü K.J., and Siegenthaler, C., 1969, Preliminary experiments on hydrodynamic movement induced by evaporation and their bear on the dolomite problem, Sedimentology- Elsevier Publishing Company, v. 12, p. 11-25.

Hudson, J.D., 1977, Stable isotopes and limestone lithification, Journal of the Geological Society of London, p. 637-658.

Ireland, H.A., 1955, Pre-Cambrian surface in northeastern Oklahoma and parts of adjacent states: American Association Petroleum Geologists Bulletin, v. 39, p. 468-483.

Johnson, K.S., 1991, Geologic Setting of the Arbuckle Group in Oklahoma, Oklahoma Geological Survey: Arbuckle Group Core Workshop and Field Trip, Special Publication, v. 91-3, 5, p. 3-7.

Keller, T. J., J. M. Gregg, and K. L. Shelton, 2000, Fluid migration and associated diagenesis in the greater Reelfoot rift region, mid-continent, U.S.A.: Geological Society of America Bulletin, v. 112, no. 11, p. 1680–1693.

King, B.D., 2013, Fluid Flow, Thermal History, and Diagenesis of the Cambrian-Ordovician Arbuckle Group and Overlying Units in South-Central Kansas, University of Kansas, Unpublished Master's Thesis, 288 p. 8-127.

Leach, D.L., and Rowan, E.L., 1986, Genetic links between Ouachita foldbelt and the Mississippi Valley-type deposits of the Ozarks: Geology, v. 14, p. 931-934.

Luczaj, J. A., Harrison, W. B., III, and Williams, N. S., 2006, Fractured Hydrothermal Dolomite Reservoirs in the Devonian Dundee Formation of the Central Michigan Basin. AAPG Bulletin, v. 90, p. 1787-1801.

Lucia, J.F., 2012, The great Lower Ordovician cavern system, in J.R. Derby, R.D. Fritz, S.A. Longacre, W.A. Morgan, and C.A. Sternbach, eds., The great American carbonate bank: The geology and economic resources of the Cambrian–Ordovician Sauk megasequence of Laurentia: AAPG Memoir 98, p. 83-111.

Lund Snee, J.-E., and M. D. Zoback, 2016, State of stress in Texas: Implications for induced seismicity, Geophys. Res. Lett., 43, doi:10.1002/2016GL070974.

Lynch, M., and Al-Shaieb, 1991, Evidence of paleokarstic phenomena and burial diagenesis in the Ordovician Arbuckle Group of Oklahoma, Oklahoma Geological Survey Circular v.92, p. 41-58.

Marsh, S., and Holland, A., 2016, Comprehensive Fault Database and Interpretive Fault Map of Oklahoma: Oklahoma Geological Survey, Open-File Report, OF2-2016, 15.

McQueen, H. S., 1931, Insoluble residues as a guide in stratigraphic studies: Missouri Bureau of Geology and Mines, Biennial Report 1929-1930, p. 102-131.

McCracken, E., 1955, Correlation of insoluble residue zones of upper Arbuckle of Missouri and southern Kansas: American Association of Petroleum Geologists, Bulletin, v. 39, p. 47-59.

McCracken, M. H., 1964, The Cambro-Ordovician rocks of northeastern Oklahoma and adjacent areas, in McHugh, J. W. (ed.), Symposium on the Arbuckle, Tulsa Geol. Soc. Digest, v. 32, p. 49-75.

McKenzie, J.A., Hsü, K.J., and Schneider, J.F., 1980, Movement of subsurface waters under the sabkha, Abu Dhabi, UAE, and its relation to evaporative dolomite genesis, SEPM Special Publication No. 28, p. 11-30.

McNamara, D. E., H. M. Benz, R. B. Herrmann, E. A. Bergman, P. Earle, A. Holland, R. Baldwin, and A. Gassner, 2015, Earthquake hypocenters and focal mechanisms in central Oklahoma reveal a complex system of reactivated subsurface strike-slip faulting, Geophysical Research Letters, 42, doi:10.1002/2014GL062730.

Moñtanez, I.P., and Read, J.F., 1992, Fluid-rock interaction history during stabilization of early dolomites, upper Knox Group (Lower Ordovician), U.S. Appalachians: Journal of Sedimentary Petrology, v. 62, n. 5, p. 753-778.

Moñtanez, I.P., 1994, Late diagenetic dolomitization of Lower Ordovician Upper Knox Carbonates: A record of the hydrodynamic evolution of the southern Appalachian Basin: American Association of Petroleum Geologists Bulletin, v. 78, p. 1210-1239.

Morgan, B.C., and Murray, K.E., 2015, Characterizing Small-Scale Permeability of the Arbuckle Group, Oklahoma, Oklahoma Geological Survey Open-File Report: OF2-2015, Norman, OK. 12, p. 1-11.

Murray, K.E., 2014, Inventory of Class II Underground Injection Control Volumes in the Midcontinent, Oklahoma Geological Survey, Shale Shaker, p. 98-106.

Murray, K.E., 2015, Class II Saltwater Disposal for 2009-2014 at the Annual-, State-, and County- Scales by Geologic Zones of Completion, Oklahoma: Oklahoma Geological Survey Open-File Report (OF5-2015), Norman, OK. p. 18.

Musgrove, M. and Banner, J.L., 1993, Regional groundwater mixing and the origin of saline fluids - Midcontinent, United States. Science 259, 1877-1882.

Northcutt, R.A., Campbell, J.A., 1995, Geologic Provinces of Oklahoma, Oklahoma Geological Survey, Shale Shaker, p. 99-103.

Overstreet, R.B., Oboh-Ikuenobe F.E., and Gregg J.M., 2003, Sequence stratigraphy and depositional facies of Lower Ordovician cyclic carbonates, Southern Missouri: Journal of Sedimentary Research, p. 421-433.

Palmer, J., Thompson, T.L., Seeger, C., Miller, J.F., and Gregg J.M., 2012, The Sauk Sequence from the Reelfoot Rift to Southwestern Missouri, in Derby, J. R., Fritz, R. D., Longacre, S. A., Morgan, W. A., and Sternbach, C. A., eds., The great American carbonate bank: The geology and economic resources of the Cambrian – Ordovician Sauk megasequence of Laurentia: American Association of Petroleum Geologists Memoir 98, p. 1013-1030.

Patterson, R.J. and Kinsman, D.J., 1982, Formation of diagenetic dolomite in coastal sabkha along Arabian (Persian) Gulf, American Association of Petroleum Geologists Bulletin, v. 66, p. 28-43.

Perry, W., Jr., 1989, Tectonic Evolution of the Anadarko Basin region, Oklahoma, United States Geological Survey Bulletin, no. 1866-A, 28, p. A1-A16.

Qing, H., and Veizer, J., 1994, Oxygen and carbon isotopic composition of Ordovician brachiopods: Implications for coeval seawater, Geochimica et Cosmochimica Acta vol. 58, p. 4429-4442.

Radke, B.M. and Mathis, R.L., 1980, On the formation and occurrence of saddle dolomite: Journal of Sedimentary Petrology, v. 50, n.4, p. 1149-1168.

Reeder, L. R., 1974, The control of potential Arbuckle hydrocarbon traps in northeastern Oklahoma by Precambrian topography: Shale Shaker, V. 24, p. 84-93.

Roedder, E., 1984, Fluid inclusions: Mineralogical Society of America, Reviews in Mineralogy, v. 12, 644 p.

Sargent, K. A., 1969, Geology and petrology of selected tectonic dolomite areas in the Arbuckle Group, Arbuckle Mountains, south-central Oklahoma. Geology. Norman, University of Oklahoma, OK: 85.

Schoenball, M., and Ellsworth, W, 2017, A systematic assessment of the spatiotemporal evolution of fault activation through induced seismicity in Ok and southern KS. Journal of Geophysical Research: Solid Earth, 122, 10,189–10,206. https://doi.org/10.1002.

Shelton, K. L., and P.M. Orville, 1980, Formation of synthetic fluid inclusions in natural quartz: American Mineralogist, v. 65, p. 1233-1236.

Shelton, K.L., Bauer, R.M.2, and Gregg, J.M., 1992, Fluid inclusion studies on regionally extensive epigenetic dolomites in southeastern Missouri: Geological Society of America Bulletin, v. 104, no. 4, p. 675-683.

Sibley, D.F., and Gregg, J.M., 1987, Classification of dolomite rock texture: Journal of Sedimentary Petrology, v. 57, p. 967-975.

Shelton, K.L., Gregg, J.M., Johnson, A.W., 2009, Replacement Dolomites and Ore Sulfides as Recorders of Multiple Fluids and Fluid Sources in the Southeast Missouri Mississippi Valley-Type District: Halogen-87Sr/86Sr-del18O-d34S Systematics in the Bonneterre Dolomite, Economic Geology, v. 104, pp. 733-748.

Sternbach, C.A., 2012, Petroleum resources of the great American carbonate bank, in J. R. Derby, R. D. Fritz, S. A. Longacre, W. A. Morgan, and C. A. Sternbach, eds., The great American carbonate bank: The geology and economic resources of the Cambrian – Ordovician Sauk megasequence of Laurentia: AAPG Memoir 98, p. 125-160.

Stoffell, B., Appold, M.S., Wilkinson, J.J., McClean, N.A., and Jeffries, T.E., 2008, Geochemistry and Evolution of Mississippi Valley-Type Mineralizing Brines from the Tri-State and Northern Arkansas Districts Determined by LA-ICP-MS Microanalysis of Fluid Inclusions, Economic Geology, v. 103, no. 7, p. 1411.

Swart, P. K., and Eberli, G. P., 2005, The nature of the d13C of periplatform sediments: Implications for stratigraphy and the global carbon cycle: Sedimentary Geology, v. 175, p. 115-130.

Swart, P.K., 2015, The geochemistry of carbonate diagenesis; the past, present and future, Sedimentology v. 62, no. 5, p. 1233-1304.

Taylor, R.D., Leach, D.L., Bradley, D.C., and Pisarevsky, S.A., 2009, Compilation of mineral resource data for Mississippi Valley-type and clastic-dominated sediment-hosted lead-zinc deposits: U.S. Geological Survey Open-File Report 2009–1297, 42 p.

Temple, B.J., 2016, Petrology and Geochemistry of the Lower Ordovician and Upper Cambrian (Arbuckle) Carbonates, NE Oklahoma and SW Missouri, Oklahoma State University, Unpublished Master's Thesis, 78 p. 1-69.

Travis, A., 1930, Oil and Gas in Oklahoma, Oklahoma County: Oklahoma Geological Survey Bulletin, No. 40-SS.

Veizer, J., Ala, D., Azmy, K., Bruckschen, P., Buhn, D., Bruhn, F., Carden, G.A., Diener, A., Ebneth, S., Godderis, Y., Jasper, T., Korte, C., Pawellek, F., Podlaha, O. G., and Strauss, H., 1999, 87Sr/86Sr, δ13C and δ18O evolution of Phanerozoic seawater, Chemical Geology, v. 161, p. 59-88.

Viets, J.G., Leach, D.L., 1990, Genetic Implications of Regional and Temporal Trends in Ore Fluid Geochemistry of Mississippi Valley-Type Deposits in the Ozark Region, Economic Geology, v. 85, 20, p. 842-861.

Walsh, F., R., Zoback, M.D., 2015, Oklahoma's recent earthquakes and saltwater disposal: Science Advances 1, e1500195.

Walters, R.J., Zoback, M.D., Baker, J.W., Beroza, G. 2016, Characterizing and Responding to Seismic Risk Associated with Earthquakes Potentially Triggered by Fluid Disposal and Hydraulic Fracturing. Seismological Research Letters. 86 (4): 1110-1118.

APPENDICES

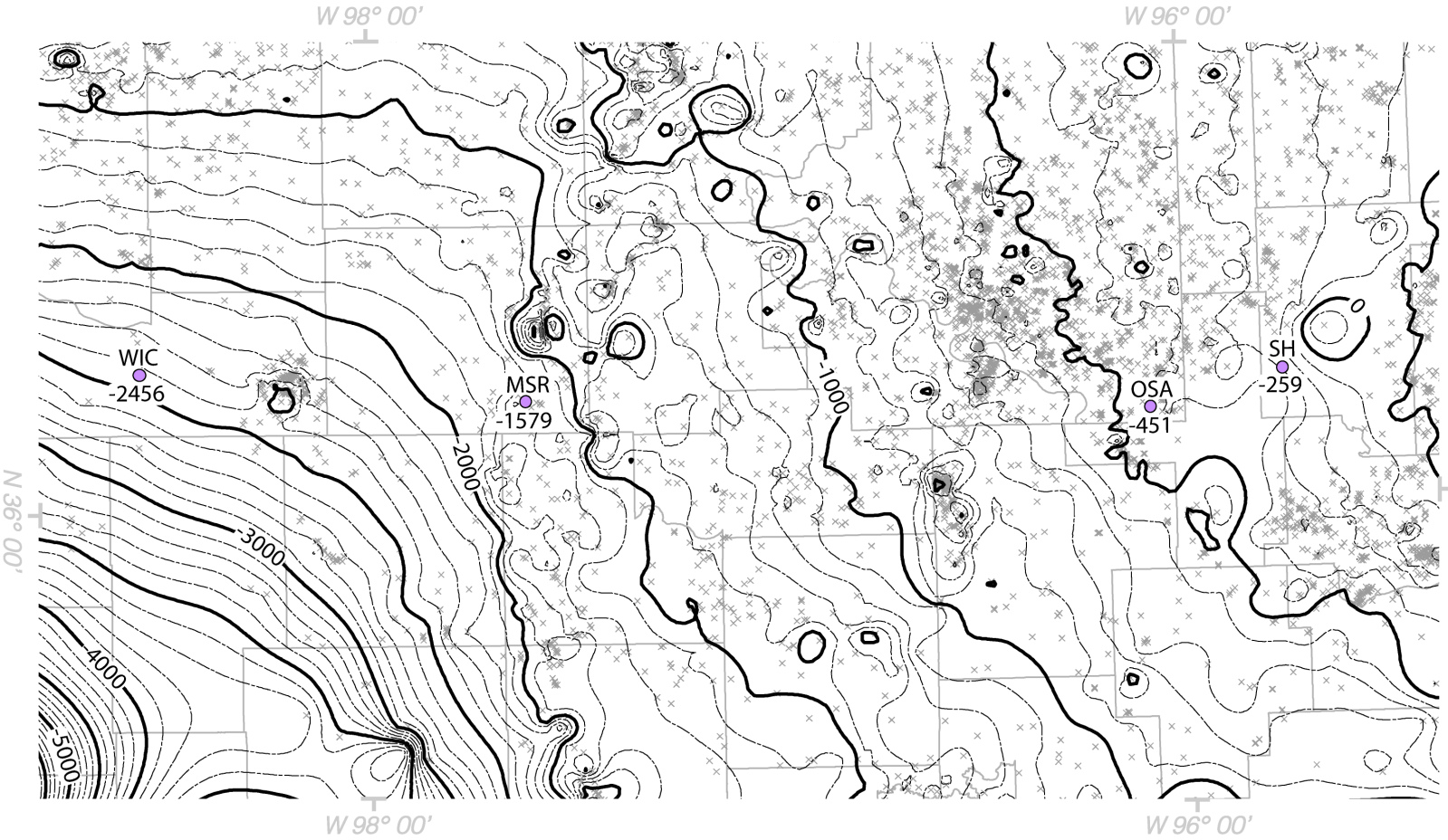

Appendix 1. *Top of Arbuckle structure map with core locations*. Formation data from IHS Enerdeq was downloaded and are shown on the map as an 'x' for each well location with a Arbuckle top. The top of the Arbuckle is shown for each cored well used in this study in meters subsea. 100m subsea contours were generated using the kriging interpolation method in Esri ArcGIS. No smoothing or top validation was performed.

Depth (m)	Lithologic Description
492.6	(LOWER ORDOVICIAN* to UPPER CAMBRIAN *Arbuckle Group)* (Shallow marine shelf with repeated subaerial exposure.) (Entire unit has dull yellow-green to pinkish-yellow fluorescence.)
492.6	(?*Cotter and Powell Fms.?)*
492.6	Dolomite. Mostly light gray to buff, medium crystalline, slightly porous; with coarsely crystalline dissolution cavity fillings and pods to tabular units of well-rounded medium-grained quartz sandstone (probably derived from unit above as cavity filling.) Locally brecciated. Sparse green clay lining cavities. Slightly porous, ~8%, no significant vugs.
494.7	Dolomite. Light to medium gray, medium to coarse crystalline, fractured by dissolution brecciation, porous to vuggy, vugs 3-30 mm across, Short zones of 25% porosity. Tight zone with light blue-gray slaking shale layers 1628.5-29.0.
499.5	Dolomite, chert, breccia, shale, sandstone. Dolomite, light gray, finely crystallic, laminated, locally grades to: shale, light greenish-gray. Contains zones of collapse breccia and cave fill, consisting of dolomite, shale, white chalky chert, soft green shale, and white medium-grained quartz sandstone. Local chert nodules. Hard.
503.4	Dolomite. Light gray, fine crystalline (microsucrosic). Probably dolomitized lime mudstone. Medium.
505.0	Dolomite, chert and shale. Dolomite, light to medium gray, fine to medium crystalline. Originally laminated and burrow-mottled. Numerous collapse breccias, common vertical and incline fractures, chert nodules and breccias. Localized green shale cavern fill at 1657.5-.9.
516.0	Dolomite. Light gray fine to medium crystalline, highly porous, vuggy, moldic, slight fracture. Thine zones of vuggy porosity >25%. Hard.
518.2	Dolomite and chert. Mostly tight, finely crystalline, originally laminated mudstone, with abundant chert nodules and cherty zones. Numerous partially fractured and vuggy zones with little matrix porosity. Scattered thin zones of oomoldic, fossil (?) moldic porosity.
540.4	Dolomite, chert, and shale. Dolomite, light gray, finely crystalline, largely dolomitized algal laminite boundstone grading down to dark brown laminated mudstone. Short intervals of intercrystalline, pelmoldic, and microvuggy porosity near top, moldic and vuggy at base. Thin shales at top, 1774.5, 1789.6, and at base. Siliceous zone throughout; and scattered large white, chalky and light gray, very hard, dense chert nodules throughout. Hard to very hard.
548.3	Dolomite, chert, and shale. Dolomite, light brownish-gray, medium crystalline oomoldic packstones(?), with interbeds of medium gray burrow-mottled wackestone. Chertified zones throughout. Dark green shale 1806.3-1807. Very hard.
551.9	Dolomite and chert, minor shale. Dolomite light gray to light brown. Tight, finely crystalline laminated mudstone; several thin zones of medium crystalline, slightly porous burrowed wackestone. Chert present in almost every foot in form of nodules, thin layers and indistinct silicified zones up to 0.2 ft thick. Shale is dark greenish-gray in the laminae and partings at 1817, 1836, 1844-45. Hard to very hard.
563.0	Dolomite, siliceous. Light to medium brownish-gray burrow mottled dolomite wackestones, mostly finely crystalline. Porous zones of finely crystalline ooid or pellet moldic packstones at 1856-1858.8, 1863-64, 1872-74.5. Very few, small chert nodules, many zones very hard, indistinctly silicified. Very hard with soft porous zones.
	Dolomite, siliceous, cyclic. Five distinct shoaling upward cycles as follows: At base is laminated to thin bedded, dark brown to light gray layers of mudstone, finely crystalline. Grades up to burrowed wackestone, fine to medium crystalline, light brownish-gray.

Appendix 2. *Digitized table of Shads 4 Lithology Descriptions (Derby, 1991)*.

Depth (m)	Lithologic Description
571.4	Upper unit is fossil and oolitic packstone, may have moldic porosity. Top may have some diagenetic terrane dissolution breccias. Chert distributed throughout as small nodules and vague silicified zones. Bases of cycles as follows: 1946.8, 1919.4, 1908.5, 1897.4, 1889.9. Hard.
593.4	Dolomite, cherty. Dolomite, light gray, fine crystalline mudstones and algal laminates, locally with medium to coarse crystalline breccias and cavity fillings. Few zones several feet thick of burrowed wackestones and oomoldic packstone. Prominent white chalky chert nodules to 0.2 ft thick scattered throughout. Local porosity in vugs, molds, and fractures, but no significant porous zones. Grades to unit below. Probably subaerially exposed diagenetic terrane. Very hard.
605.2	Dolomites, locally cherty. Light gray to dark brown finely crystalline, tight, mudstones and algal laminates. Thin zones of burrowed wackestones. Sparse small light gray chert nodules. No porosity. Hard.
615.8	(?Top of *Jefferson City FM.?)*
615.8	Dolomite. Light tan to brown, fossiliferous, oolitic, porous packstones, medium crystalline. Insignificant chert. Few thin brown intervals of brown mudstone. Recognizable large gastropods (*Helicotoma?*) at 2025.1 and 2048.9. Oomoldic and fossil moldic porosity, locally enhanced by fractures and vugs. Hard.
	Dolomite, cherty. Shoaling upward cycles of thin slightly porous fossiliferous pelletal or oolitic packstone(?) at top; light tan to brown, slightly shaly mudstones at base, mudstone 3-5 ft thick, porous intervals 1 or 2 ft. Dark brown, oil stained mudstones in lower 634.9 two cycles. Cherty or siliceous intervals; 2092-93.3, 2100-2101, 2104.5-2105.4, 2110.7-2112; nodules at 2111.4, 2114.5, 2121.4 (oil shows, leached), 2134.0, 2140-41. Oil stained sandstones, 0.2 ft thick at 2142.2, 2135.1. Shaly zones at 2095.0-2096.1, 2104.4.5, 2108.6-09.1-
655.7	Dolomite, cherty. Light to dark brown, tight mudstones and rubbly thrombolitic slightly porous wackestones; discontinuous cherty throughout. Thin zones of algal laminates appear leached. Vuggy and fracture porosity in wackestone some coarse crystalline vug fillings. Hard.
662.5	Sandstone, dolomitic. White, very fine grained to fine grained, well rounded, well sorted, dolomite cemented, tight. Hard.
662.9	Chert and dolomite. Siliceous to chertified cycles of algal laminates to rubbly thrombolitic dolomites, to oolitic, pelletal grainstones. Greater than 50% chert, mostly as replacement of dolomite textures, fewer distinct nodules (see fluorescent list). Chert nodules chalky to light blue-gray and translucent, commonly with moldic porosity. Some cherty zones are agate and silicified ooids. Many zones of dissolution breccias. Generally, tight rock with vuggy and fracture porosity. Locally, distinct stromatolitic structures.
680.5	Sandstone, white fine grained, poorly sorted and well rounded, pebbly at top with dolomite and phosphatic clasts, dolomite cemented. (Possibly other thin zones of sandstone, difficult to distinguish on unslabbed core from silicified granular dolomite!) Thin (0.1-0.2 ft) dark shale intervals at 2190, 2195, 2199.8, 2221.8, and 2238.8. Extremely hard.
684.2	Dolomite, cherty. Medium brown to medium gray porous thrombolitic dolomite, partially silicified with chert nodules and siliceous zones, and zones of dissolution breccia. Much like unit above but less chert. Thin shaly mudstone zones at 2265, 22278-79, 2287, 2292-94, and 2328. Local vuggy porosity to 30%, vugs to 2 cm across. Sparse very thin quartz sandy zones. Extremely hard to cherty layers to moderately hard in porous dolomite units (see list of porosity zones).
711.7	Dolomite, cherty. Medium gray to dark brownish-gray finely crystalline dolomite mudstone, most very tight with 1-2 ft zones of algal laminates, planar stromatolites and thrombolites. Discontinuous vuggy and fracture porosity. Thin (0.1-0.2 ft) zones of very hard, brittle chert, mostly brecciated and adjacent to quartz and dolomite lined vugs. Some vugs extend width of core and 3 cm high. Zone of horizontal fenestral porosity (20%) at 2365.4-2367 in planar stromatolites. Hard to locally extremely hard, much "twisted off" core.
725.1	(?*Roubidoux Fm.)*

Appendix 2 (cont'd). *Digitized table of Shads 4 Lithology Descriptions (Derby, 1991)*.

Depth (m)	Lithologic Description
725.1	Dolomite, cherty. Light to medium gray, fine to coarse crystalline, interbedded tight and porous. Thrombolitic, stromatolitic, and ?grainstone dolomite. Moderate porosity and permeability at top, increasing to zones of >20% porosity towards base. Thin (0.1-0.2 ft) intervals of light bluish-gray chert at 2476.5-2479, 2505.3-2510.8. Porous coarse crystalline dolomites locally partially silicified. Coarsely crystalline slightly porous dolomites strongly resemble sandstones but generally lack quartz sand. Thin (0.1-0.2 ft) dark shaly layers of 2395, 2419.8, 2458, 2494.7, 2497.3, and 2529.7. Thin sandy zones at 2388.6-.7 and 2411.0-.3. Hard to very hard. Extremely hard chert zones at 2402, 2414, 2428, 2447.0-.3. Hard to very hard. Extremely hard chert zones at 2402, 2414, 2428, 2447- 50, 2457 (breccia), 2509-2511, and 2522-23. Indefinite lower contact
771.1	Dolomite and sandstone. Little to no chert. Dolomite, light gray, medium to coarse crystalline, relatively tight, thrombolitic and stromatolitic. Interbedded sandstone and sandy interval 0.5-1.5 ft thick, white to light brow (oil stained), medium to coarse grained. Mostly fairly tight rock. Sandstone at 2530.8-2531.5,2533.0-.8, 2534.6-35.5,2550.6-2552,2561-2562.6. Highly siliceous below 2552. Thin chert at 2544.8. Hard.
782.6	Dolomite, sandy. Dolomite, light gray, interbedded tight fine crystalline mudstone and porous coarse crystalline, vuggy planar stromatolites or recrystallized fenestral mudstones. Thin lenticular sandy dolomite zones throughout, plus thin sandstone beds at 2580.9 81.1, 2593.9-94.2, 2595.0-.2, 2597.5-.8, 2597.4-98.1,2601.2-.5, and 2602.0-.3. Few thin chert nodules and siliceous zone. Scattered large vugs. Hard.
797.1	*(?Gasconade Fm.?)*
797.1	Dolomite, cherty. Dolomite light gray to light brown medium to coarsely crystalline, porous with thin zones of medium bluish-gray very dense chert, typically fractured and/or vuggy. Macro-porosity associated with chert and vugs but thick intervals of good intercrystalline porosity. Highly siliceous chertified dolomite zones throughout. Hard.
816.2	Chert, dolomitic. Light gray to brown (oil stained) chertified dolomite algal and thrombolitic mudstone; few white to gray chert nodules. Vuggy and fractured; tight matrix down to 2686, microporous oil stained 2686 to base.
821.6	Cherty, dolomitic. Light to dark bluish- to brownish-gray chertified dolomite mudstone with nodules of white chalky chert and hard dense dark gray chert. White dolomite crystals fill vugs and line cavities. Thin zones of brecciated chert. Vugs to 2cm high extend across core. Matrix tight to slightly porous (some intervals salt encrusted). Mostly crudely laminated. Gradational to unit below. Very hard.
840.3	Chert and dolomite. Light brownish-gray to medium gray, mostly porous chertified burrowed dolomite mudstones, algal laminates, and hemispherical stromatolites. Nodules of white to dark gray brecciated dense chert. Irregularly interbedded intervals of less siliceous medium to coarse crystalline dolomite. Numerous quartz-crystal-lined vugs, some extending entirely across core and 1-2cm high. much intercrystalline microscopy and vuggy macroporosity. Zones of extremely high permeability, cavernous vuggy porosity at 2784.3-.7, 2789.4-90.2, 2791-92.3. Zone of extremely hard dense chert 2785.5-2788.5 Very hard.
862.7	*(?Gunter Sandstone Member of Gasconade Fm.?)*
862.7	Dolomite, sandstone, and chert. Dolomite, medium brownish-gray, medium to coarsely crystalline, burrow-mottled and algal laminated mudstone; locally siliceous grading to chertified dolomite (no distinct chert nodules). Sand occurs as many thin lenses in dolomite, and thicker beds of white, medium grained well-rounded sand at 2737-38.7, 2846.8-2849.4, 2851.6-2854, 2858.9-2859.8. Transitional contact to unit below. Hard.
872.9	Dolomite, siliceous. Medium to dark gray, medium to coarse crystalline laminated to burrow-mottled siliceous mudstone; thin dark shaly zones and sandstone stringers. Generally tight with scattered small vugs, dolomite or chert filled. Hard.
876.2	Dolomite and sandstone, interbedded. Dolomite medium to dark gray, medium crystalline tight, siliceous, laminated to slightly burrowed mudstone. Interbeds of white to light gray with brown stringers medium-to coarse-grained quartz sandstone, tight, at 2874.6- 75.2, 2878.9-79.1, 2881.0-83.8. Hard.

Appendix 2 (cont'd). *Digitized table of Shads 4 Lithology Descriptions (Derby, 1991).*

Depth (m)	Lithologic Description
879.0	Dolomite, siliceous to chertified. Medium to dark gray, medium crystalline laminated and burrow-mottled. Tight with mostly isolated open or dolomite-filled vugs. Thin vuggy zones of sulfide mineralization 2885-2897. Dolomite all very hard, siliceous, locally converted to dense chert. Very hard.
884.6	Sandstone, dolomite, and shale. Sandstone, white to medium gray, medium to coarse grained, locally pebbly with thin intercalation of dolomite and shale. Dolomite, light brownish-gray, burrow-mottled and medium crystalline mudstone, beds 0.4-1.0 ft thick. Shale dark greenish-gray, thin laminae to unites 0.3 ft thick. Hard.
887.6	Dolomite and shale, sandy. Dolomite, light brownish-gray, medium crystalline, burrow-mottled mudstone. Shale, light to medium gray laminae to units 0.2 ft thick. Floating quartz sand throughout; few thick sand lenses. Hard.
888.8	Sandstone. White to light greenish-gray, medium to coarse grained, locally fine pebbles. Slightly porous (core salt coated). Hard.
889.6	Dolomite, shale, and sandstone, interbedded. Dolomite, medium crystalline, light gray to dark brownish-gray, burrow-mottled to laminated mudstone. Thin interbeds of shale or sandstone <0.5ft thick. Sandstone as above. Shale, light to dark greenish-gray with sparse small fossil fragments. Trilobite fragments at 2919. Pebbly, weathered disconformity zone at 2932-33. Moderate to hard.
895.9	*(Basal Sandstone; "Reagan Fm.")*
895.9	Sandstone, locally shaly. White to light brown, fine to very coarse grained, locally with fine pebbles of adjacent lithologies. With thin shaly laminae and shale beds as above <0.2 ft. Moderate to hard.
898.2	Sandstone, shale, and mudstone. Fine to very fine-grained sandstone and mudstone, light gray to medium brown with laminae and thin interbeds of greenish gray shale. Locally burrowed. Transitional contact. Moderate to hard.
901.3	Sandstone, locally shaly. White, light brown to medium gray, medium to very coarse grained and fine pebbly, locally highly porous. Brown zones appear oil stained but no cut and no fluorescence. Mostly quartz with pebbles and grains of adjacent lithologies. Shale zones, as above, at 2964.3-.9, 2966.7-67.2, 2973.4-.5. Horizontal bedding. Moderate.
908.3	Sandstone, arkosic. Light to dark brown. Fine- to very coarse-grained and pebbly arkosic sandstone, derived from underlying porphyritic andesite with thin fine-grained to slightly shaly layers at 0.5-0.2 ft. Horizontal bedding. Moderately hard.
911.0	Arkosic sandstone. Dark brownish-gray, fine- to coarse-grained, poorly sorted arkosic sandstone with faint dark horizontal laminae and irregular vertical burrows or root remains. Transitional lower contact. Hard.
911.7	Arkosic sandstone. Light gray to light red-brown grading down to medium to dark reddish-brown; fine to coarse grained with very thin horizontal dark shaly laminae. Increasingly pebbly toward base. From 3010 to 3011.5 are discontinuous layers of pebbles to 2 cm across including white quartzitic sandstone, chert, shale, and andesite. Possibly a volcanic agglomerate. Hard.

Appendix 2 (cont'd). *Digitized table of Shads 4 Lithology Descriptions (Derby, 1991).*

API	WellName	Operator	County	Latitude	Longitude	Legal Location	WellType	KB Depth (m)	Total Depth (m)	Spud Date	Completion Date	Source
3504720421	Meisner MH 2	Tenneco Oil Company	Garfield	36.2300429	-97.6151158	10-20N-4W	OIL WELL	322	2384	7/29/68	8/30/68	IHS/OCC
3511330447	Osage C1	Texaco Incorporated	Osage	36.1927138	-96.0843594	24-20N-11E	DRY & ABANDONED WELL	306	1125	6/4/65	9/21/65	IHS/OCC
3509300025	Wichert HC1	Gulf Oil Corporation	Major	36.2915833	-98.5620723	14-21N-13W	ABANDONED GAS WELL	422	2907	7/13/59	12/16/59	IHS/OCC
3513124261	Shads 4	Amoco Prod Co	Rogers	36.265765 (est.)	-95.760544 (est.)	25-21N-14E	OBSERVATION WELL	236	1058	unknown	unknown	IHS/OCC

Appendix 3. *Well details.*

Sample ID	Location	Petrographic Description	Lithology Classification (Dunham)
SH 498m	Rogers Co., OK	Unimodal, very fine to finely crystalline, planar-s dolomite. Possible chert.	Bioturbated, dolomitic mudstone
SH 501m		Unimodal, finely crystalline, planar dolomite with fracture filling (void filling) nonplanar dolomite cement. Considerable chert is present.	Cherty, dolomitic packstone
SH 564m		Unimodal, very fine to finely crystalline, planar-e to planar-s dolomite.	Bioturbated, vuggy, dolomitic mudstone
SH 604m		Polymodal, fine to medium crystalline planar-s to nonplanar dolomite with coarse, unimodal, nonplanar vug filling (void filling) dolomite cement.	Vuggy, dolomitic mudstone with some fractures
SH 637m		Nodular, oolitic chert	Nodular, oolitic chert
SH 638m		Polymodal, very fine to finely crystalline, planar-s dolomite with vug filling (void filling) unimodal, medium to coarsely crystalline, nonplanar dolomite cement.	Vuggy, mottled, dolomitic wackestone
SH 678m		Unimodal, very fine to finely crystalline, planar-s dolomite accompanied by a cherty oolitic grainstone.	Cherty, oolitic grainstone to finely laminated, bioturbated, dolomitic mudstone
SH 682m		Very fine to finely crystalline, unimodal, planar-s dolomite vug filling (void filling), medium to coarsely crystalline, nonplanar dolomite cement.	Vuggy, dolomitic mudstone with minor fractures
SH 682m		Very fine to finely crystalline, unimodal, planar-s dolomite.	Dolomitic, finely laminated mudstone with some minor fractures
SH 718m		Very fine to medium crystalline, polymodal, planar-s dolomite with large vug filling polymodal, nonplanar dolomite with some distributed chert.	Fractured, dolomitic wackestone to packstone with some chert
SH 799m		Unimodal, medium crystalline, planar-e dolomite with mimically replaced allochems (ooids).	Vuggy dolomitic mudstone
SH 805m		Polymodal, medium-coarse crystalline planar-s and nonplanar dolomite with mimically replaced allochems (ooids).	Crystalline carbonate or fractured, fenestral, dolomitic packstone to grainstone (organic lean)
SH 882m		Unimodal, very finely to finely crystalline, planar-e to planar-s dolomite with fracture filling (void filling), unimodal, nonplanar dolomite cement.	Vuggy, dolomitic mudstone or finely crystalline dolomite
OSA 1036m	Osage Co., OK	Medium crystalline, polymodal, planar-e to planar-s dolomite to nonplanar dolomite.	Medium crystalline dolomite
OSA 1039m		Medium crystalline, unimodal, planar-s to nonplanar dolomite.	Medium crystalline dolomite
OSA 1042m		Medium crystalline, unimodal, planar-e to planar-s dolomite	Medium crystalline dolomite
OSA 1044m		Medium to coarsely crystalline, polymodal, planar-s to nonplanar dolomite	Vuggy, medium to coarsely crystalline dolomite
OSA 1048m		Transition from sandstone to dolomite. Fine-medium crystalline, polymodal, planar-s to nonplanar dolomite.	Fine-medium crystalline, sandy dolomite
OSA 1048m		Sandy dolomite to sandstone w/ dolomitic cement (quartz-rich some feldspar and polymorph quartz, chert rock frags (<1-2%)).	Quartz arenite to feldspathic sandstone. Sandy, crystalline carbonate
MSR 1904m	Garfield Co., OK	Unimodal, planar-s, finely crystalline dolomite	Finely laminated, organic-lean dolomitic mudstone or finely crystalline dolomite
MSR 1907m		Unimodal, finely crystalline, planar-e to planar-s dolomite (molds…) with fracture filling (void filling) unimodal, coasrely crystalline, nonplanar dolomite cement.	Finely laminated, fractured, organic-lean mudstone or finely laminated crystalline dolomite
MSR 1907m		Unimodal, very finely to finely crystalline planar-e to planar-s dolomite with mimically replaced allochems (nonskeletal).	Finely laminated, organic lean mudstone to brecciated, interclastic wackestone
MSR 1914m		Unimodal, very finely to finely crystalline, planar-e to planar-s dolomite with vug filling (void filling) unimodal, medium to coarsely crystalline, nonplanar dolomite cement.	Fractured, bioturbated, vuggy organic lean mudstone, interclastic wackestone
MSR 1914m		Unimodal, planar-s dolomite with channel/fracture filling (void filling) unimodal, coarsely crystalline, nonplanar dolomite cement.	Fractured, vuggy, organic lean mudstone to brecciated, vuggy, interclastic wackestone
MSR 1919m		Unimodal, very fine to finely crystsalline planar-s dolomite with mimically replaced allochems (micritic texture)	Finely laminated, organic-lean pelleted/peloidal mudstone or finely crystalline dolomite
MSR 1923m		Unimodal, very finely crystalline planar-e to planar-s dolomite.	Crinkly laminated, organic lean mudstone or bacterial laminates
MSR 1924m		Unimodal, finely crystalline, planar -e to planar-s dolomite with fracture filling (void filling) unimodal, coarsely crystalline nonplanar dolomite cement.	Fractured, vuggy, organic lean mudstone
MSR 1929m		Very fine-finely crystalline, unimodal, planar-s dolomite with some sandy dolomite.	Bioturbated, peloidal wackestone
MSR 1929m		Unimodal, planar-e to planar-s, finely crystalline dolomite with vug filling (void filling) nonplanar, medium to coarse crystalline dolomite cement.	Organic lean, vuggy mudstone
MSR 1930m		Very fine-finely crystalline, unimodal, planar-s dolomite.	Bioturbated mudstone
MSR 1935m		Polymodal, planar-s, fine-medium crystalline dolomite with some nonplanar dolomite fill (frags) allochem replaced dolomite.	Bioturbated, slightly fossiliferous mudstone to wackestone

Appendix 4. *Lithologic and petrographic core descriptions .*

Sample ID	Location	Petrographic Description	Lithology Classification (Dunham)
WIC 2883m	Major Co., OK	Very fine crystalline, unimodal, planar-e to planar-s dolomite.	Micritized dolomite mudstone
WIC 2885m		Very finely crystalline, unimodal, planar-s sandy dolomite.	Dolomitized sandy wackestone to mudstone
WIC 2899m		Fabric destructive, polymodal planar-e to planar-s dolomite (allochem replaced?) with planar void filling saddle dolomite cement.	Skeletal/peloidal wacketsone to packstone
WIC 2904m		Very fine to finely crystalline, unimodal, planar-s dolomite.	Finely-laminated, graded dolomitic mudstone to wackestone
WIC 2904m		Very fine-to finely crystalline, unimodal, planar-e to planar-s dolomite.	Laminated (sandy?) dolomitic mudstone with some vertical fractures
WIC 2905m		Unimodal, planar-e to planar-s, medium crystalline dolomite with mimic replacement fabrics.	Fabric destructive…medium crystalline dolomite with some laminations and fractures. May have been a skeletal wackestone to packstone.
WIC 2906m		Dolomitized mudstone to wackestone. Fine-medium crystalline, unimodal planar-e to planar-s, fabric non-destructive dolomite.	Laminated to highly bioturbated, pelleted, mudstone to wackestone

Appendix 4 (cont'd). *Lithologic and petrographic core descriptions.*

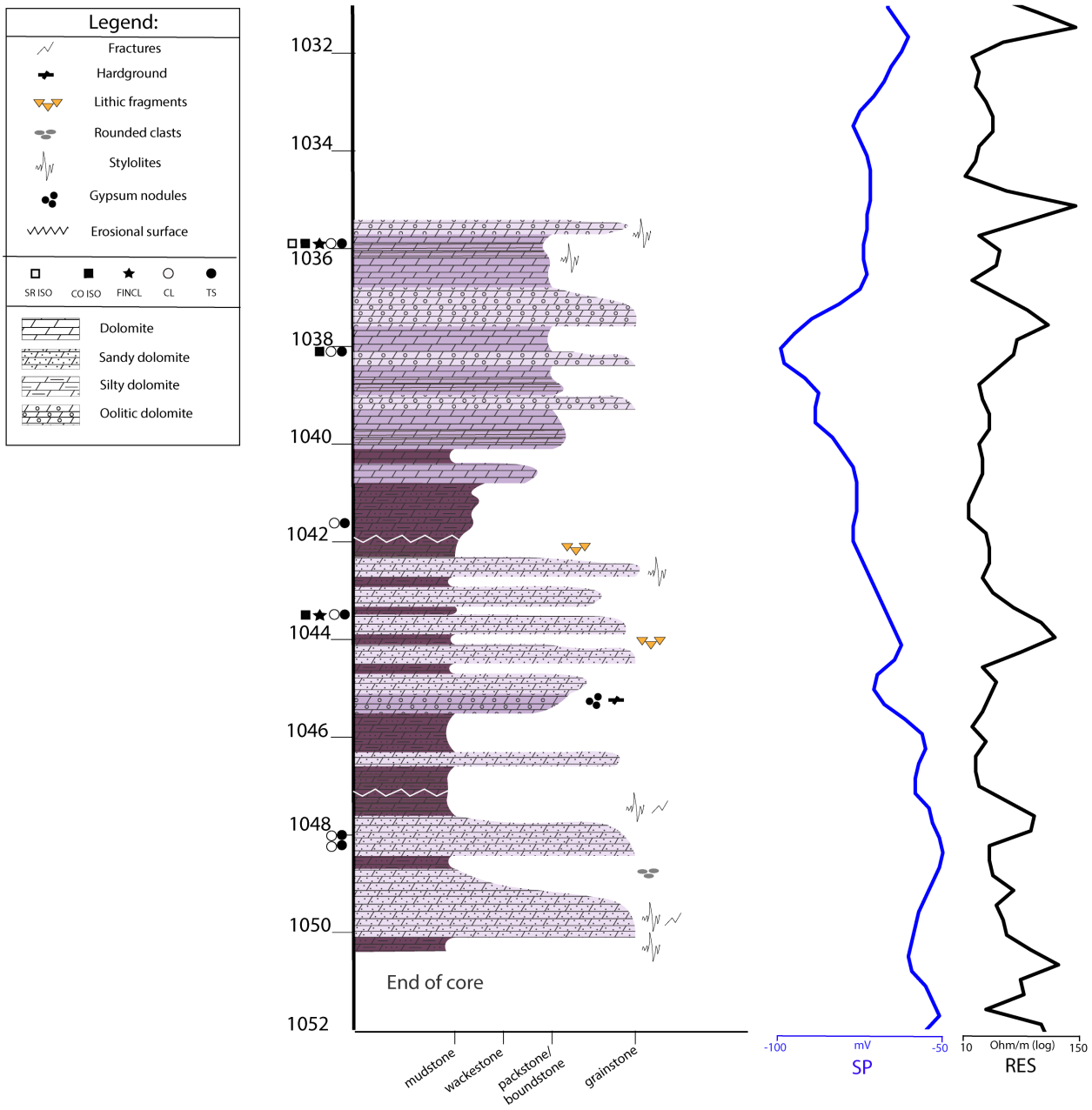

Appendix 5. *Osage C1 core graphic with wireline log.*

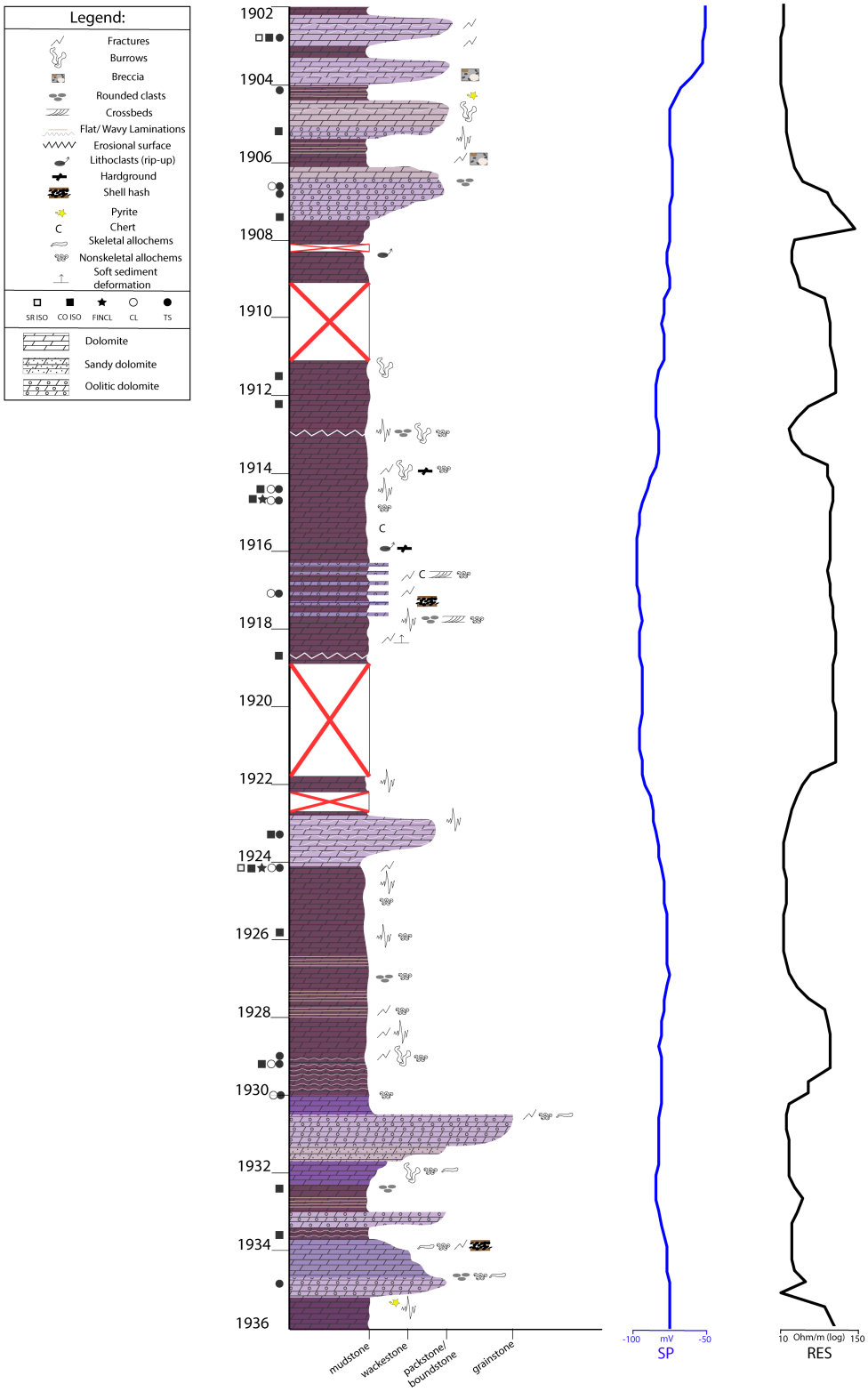

Appendix 6. *Meisner MH2 core graphic with wireline log.*

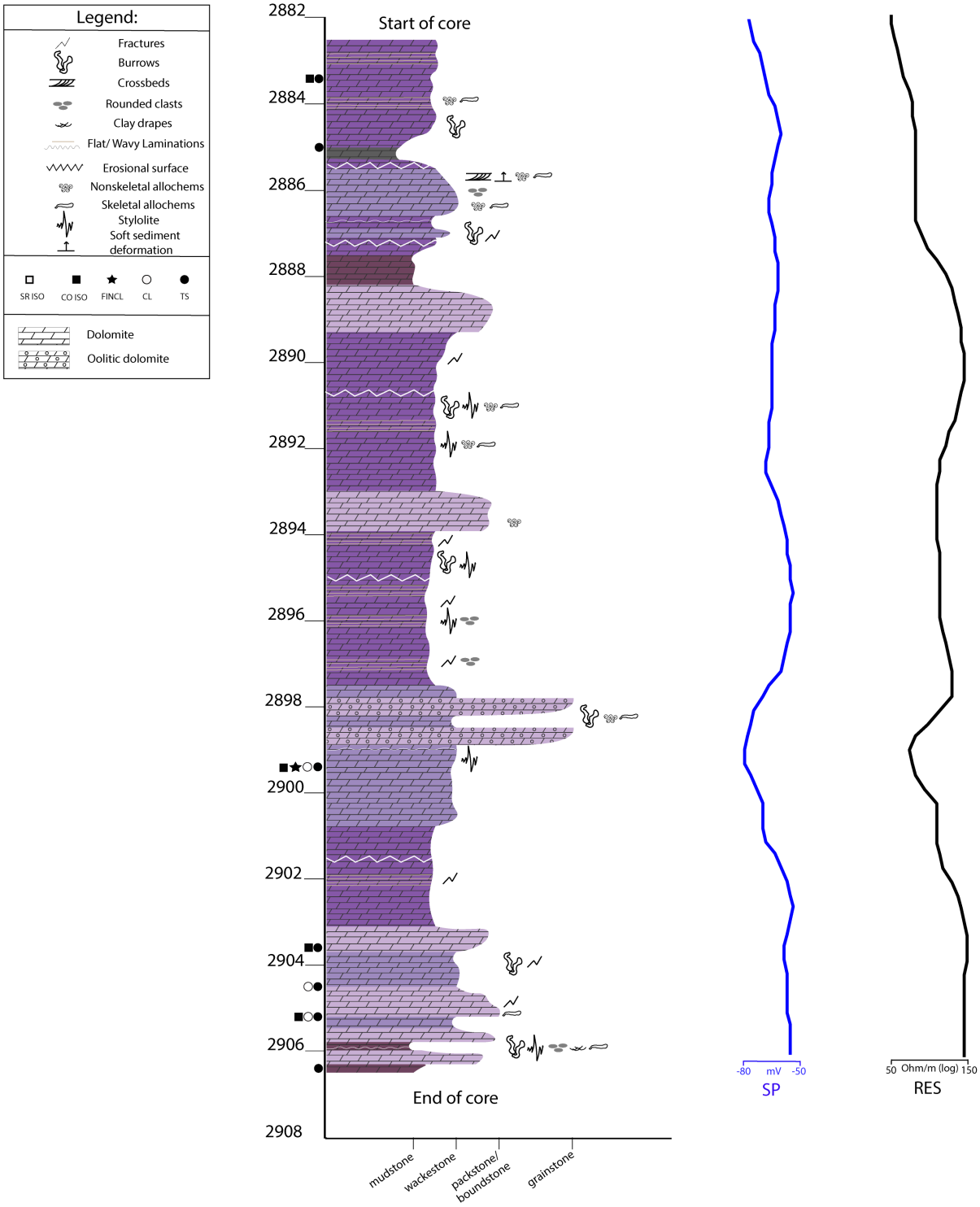

Appendix 7. *Wichert 1 core graphic with wireline log.*

Core ID	Chip/Inclusion ID	Original Assemblage ID	FIA Type	Run 1		Run 2		
				Tm	*Th*	*Tm*	*Th*	*Te*
	OSA3399 C1							
OSA3399	A	2	Primary		126.9			
OSA3399	B	2	Primary	-24.6		-23.3		
OSA3399	C	2	Primary		112.1			
OSA3399	D	2	Primary		121.1			
OSA3399	E	2	Primary	-21.7		-22.2		
OSA3399	F	2	Primary		98.7			
OSA3399	G	1	Primary	-22.7	113.5	-22.9		
OSA3399	H	2	Primary		126.0			
OSA3399	I	1	Primary		114.0			
OSA3399	J	2	Primary	-24.3		-23.5		-44.3
OSA3399	OSA3399 C2							
OSA3399	A	1	Primary		114.3			
OSA3399	B	2	Primary	-27.3	120.0			
OSA3399	C	3	Primary	-23.4	123.8			
OSA3399	D	2	Primary		120.0			
OSA3399	E	2	Primary		110.0			-40.0
MSR6282	MSR6282 C1							
MSR6282	A1	1	Primary		104.6		105.5	
MSR6282	A2	1	Primary		101.8			
MSR6282	A3	1	Primary		114.4		124.9	
MSR6282	A4	1	Primary					
MSR6282	A5	1	Primary					
MSR6282	A6	1	Primary		105.2		105.5	
MSR6282	B4	1	Primary		105.5			
MSR6282	B3	1	Primary		105.5			
MSR6282	B1	1	Primary		104.8			
MSR6282	C	1	Primary		108.1			
MSR6282	D	1	Primary		107.2			
MSR6282	E	1	Primary		111.9			
MSR6282	MSR6282 C2							
MSR6282	A	1	Primary		110.8		109.6	
MSR6282	B	1	Primary		96.1		99.4	
MSR6282	C	1	Primary	-38.9	91.6	-32.0	93.4	
MSR6282	D	2	Primary		105.4		107.3	
MSR6282	F	2	Primary		94.5			
MSR6282	G	2	Primary		105.4		99.4	
MSR6282	H	2	Primary		116.7		118.2	
MSR6282	I	2	Primary		99.4			

Appendix 8. Individual fluid inclusion microthermometry data.

Core ID	Chip/Inclusion ID	Original Assemblage ID	FIA Type	Run 1		Run 2		
				Tm	*Th*	*Tm*	*Th*	*Te*
MSR6282	MSR6282 C3							
MSR6282	A	1	Primary	-35.7	102.4		102.2	
MSR6282	B	3	Primary	-17.5	121.3		122.8	-40.2
MSR6282	E	2	Primary	-26.5	106.4		109.1	
MSR6282	F	2	Primary		122.8		128.4	
MSR6282	G	2	Primary		102.4		109.1	
MSR6282	H	3	Primary	-21.1	122.8		119.6	
OSA3424	OSA3424 C1							
OSA3424	A	1	Primary	-21.9	165.6	-20.8	159.4	-34.5
OSA3424	B	2	Primary		106.3	-20.5	119.1	
OSA3424	D	2	Primary			-22.2		
OSA3424	E	1	Primary		161.1	-23.9	130.0	
OSA3424								
OSA3424	OSA3424 C2							
OSA3424	A	1	Primary	-17.7	151.9			-40.0
OSA3424	B	1	Primary	-20.4	156.7			
OSA3424	D	2	Primary	-22.1	95.9			
SH2893	SH2893 C1							
SH2893	A	1	Primary	-22.6	130.1		130.8	-40.0
SH2893	B	1	Primary		113.4		112.8	
SH2893	SH2893 C2							
SH2893	A	1	Primary	-25.9	130.8			-40.0
SH2893	B	2	Primary	-23.7				
SH2893	C	2	Primary		132.8			
SH2893	D	3	Primary		117.7			
SH2893	E	3	Primary		108.7			
SH2893	F	3			120.4			
SH1642	SH1642 C3							
SH1642	A	1	Primary	-22.3	97.9		98.8	-40.0
SH1642	B	1	Primary	-22.5	105.6		105.9	
SH1642	C	2	Primary	-22.6	90.8			
SH1642	SH1642 C2							
SH1642	A	1	Primary	-17.6	110.8			
SH1642	B	1	Primary	-18.1	103.5			
SH1642	C	2	Primary	-20.2	84.7			
SH1642	D	2	Primary		99.1			
SH1642	SH1642 C4							
SH1642	A	1	Primary	-24.1	129.4			
SH1642	C	2	Primary	-22.2	155.0			
SH1642	D	2	Primary	-21.0	130.1			
SH1642	E	3	Primary	-18.0	117.0			

Appendix 8 (cont'd). Individual fluid inclusion microthermometry data.

Core ID	Chip/Inclusion ID	Original Assemblage ID	FIA Type	Run 1		Run 2		
				Tm	*Th*	*Tm*	*Th*	*Te*
SH1642	F	3	Primary		117.3			
SH2237	SH2237 C4							
SH2237	A	1	Primary	-23.2	136.5		128.4	-40.8
SH2237	B	1	Primary		131.0		130.0	
SH2237	C	2	Primary	-17.3			109.8	
SH2237	D	2	Primary	-20.0			108.7	
SH2237	E	2	Primary				113.0	
SH2237	F	2	Primary				111.7	
SH2237	SH2237 C2							
SH2237	A	1	Primary	-14.5	99.1	-22.9		-40.1
SH2237	B	2	Primary	-21.3	101.8			
SH2237	C	2	Primary					
MSR6313	MSR6313 C2							
MSR6313	A	1	Primary	-23.0	128.8			
MSR6313	B	1	Primary		102.5			
MSR6313	C	2	Primary	-15.5	99.2			
MSR6313	D	1	Primary		110.0			
MSR6313	E	2	Primary	-23.5	146.4			
MSR6313	F	1	Primary	-23.2	116.1		123.9	
MSR6313	G	3	Primary	-24.1	114.1			
MSR6313	MSR6313 C3							
MSR6313	1	1	Primary		90.2			
MSR6313	2	1	Primary	-18.8	79.9			
MSR6313	3	1	Primary	-19.1	85.6			
MSR6313	4	1	Primary	-20.2	94.5			
MSR6313	5	1	Primary	-23.2	99.7			
WIC9512	WIC9512 C2		Primary					
WIC9512	1	4	Primary	-21.9	130.8			
WIC9512	2	2	Primary	-20.5	124.8			
WIC9512	3	2	Primary		111.1			
WIC9512	4	3	Primary	-21.5	131.1			
WIC9512	5	1	Primary	-21.9	120.0			
WIC9512	6	1	Primary	-22.5	110.0		143.4	
WIC9512	7	2	Primary	-22.9	134.6			
WIC9512	8	4	Primary	-18.8	100.0			
WIC9512	WIC9512 C1							
WIC9512	A1	2	Primary	-23.3				
WIC9512	A4	1	Primary	-20.0				
WIC9512	A5	1	Primary	-21.7				
WIC9512	A6	1	Primary	-20.0	125.5			
WIC9512	A7	2	Primary	-20.2	118.9			

Appendix 8 (cont'd). Individual fluid inclusion microthermometry data.

Core ID	Chip/Inclusion ID	Original Assemblage ID	FIA Type	Run 1		Run 2		
				Tm	*Th*	*Tm*	*Th*	*Te*
WIC9512	A8	2	Primary		105.5			
WIC9512	A9	2	Primary		147.9			
WIC9512	B1	1	Primary	-20.0	133.8			
WIC9512	B2	1	Primary	-25.1	114.1			
WIC9512	B3	2	Primary	-19.8	123.9			
WIC9512	B4	2	Primary	-18.3	116.7			
WIC9512	B5	2	Primary	-17.6	126.6			

Appendix 8 (cont'd). Individual fluid inclusion microthermometry data.

VITA

Phillip Anthony Bailey III

Candidate for the Degree of

Master of Science

Thesis: DIAGENESIS OF THE ARBUCKLE GROUP IN NORTHEASTERN AND NORTH-CENTRAL OKLAHOMA, U.S.A.

Major Field: Geology

Biographical:

Education:
Graduated from First Colonial High School, Virginia Beach, Virginia in May 2006.

Completed the requirements for the Bachelor of Science in Ocean, Earth, and Atmospheric Science from Old Dominion University, Norfolk, Virginia, in December 2011.

Completed the requirements for the Master of Science in Geology at Oklahoma State University, Stillwater, Oklahoma in December, 2018.

Experience:
Employed by Old Dominion University Research Foundation as a paleoclimate laboratory technician from 2009 to 2012; employed by Nomac Services as a field geologist/mudlogger from 2012 to 2014; employed by Chesapeake Energy Corporation as a geophysical technician from 2014 to 2015; employed by Oklahoma Corporation Commission as a regulatory manager/contract geologist from 2015 to present.

Professional Memberships:
Oklahoma City Geological Society
Geological Society of America
American Geophysical Union
American Association of Petroleum Geologist
Houston Geological Society